The Effects of Resistance Endurance Training on Muscle Architecture and Stem/Progenitor Cell Populations in a Murine Model of Rhabdomyosarcoma

Olivia Sanders

Thesis submitted to the University of Ottawa in Partial Fulfillment of the requirements for the degree of Master of Science – Human Kinetics

School of Human Kinetics

Faculty of Health Sciences

University of Ottawa

Table of Contents

Acknowledgements

I would like to thank Dr. Michael De Lisio for presenting me the opportunity to become a member of his fantastic lab and pursue my MSc at the University of Ottawa. His passion and drive to continuously push the boundaries of our collective understanding while at the same time providing the room in his lab for personal and professional growth are truly remarkable. Thank you Dr. De Lisio for affording me outstanding mentorship and for your kindness and understanding of the difficulties associated with beginning and finishing a master's degree during the Covid-19 pandemic. Your thoughtfulness and consideration during these extremely difficult past 2 years did not go unnoticed.

A special thank you to all the members of the De Lisio lab that supported me over the past 2 years. Your guidance and friendship were instrumental in helping me through these past 2 years.

To Dr. Pascal Imbeault and Dr. Nadine Wiper-Bergeron, a giant thank you for agreeing to be members of my thesis advisory committee and offering me exceptionally useful feedback that helped strengthen the integrity of my project and helped me stay on track during my MSc.

I am extremely grateful to my wonderful family (Tim, Gaby, Julia) for their unconditional love and support. I could not have undertaken this journey without you all. Finally, I would like to express my deepest gratitude to my Nana, Dorothy Sanders, who taught me that it's never too late to embark on the pursuit of knowledge and chase your dreams. You are my heart.

General Abstract

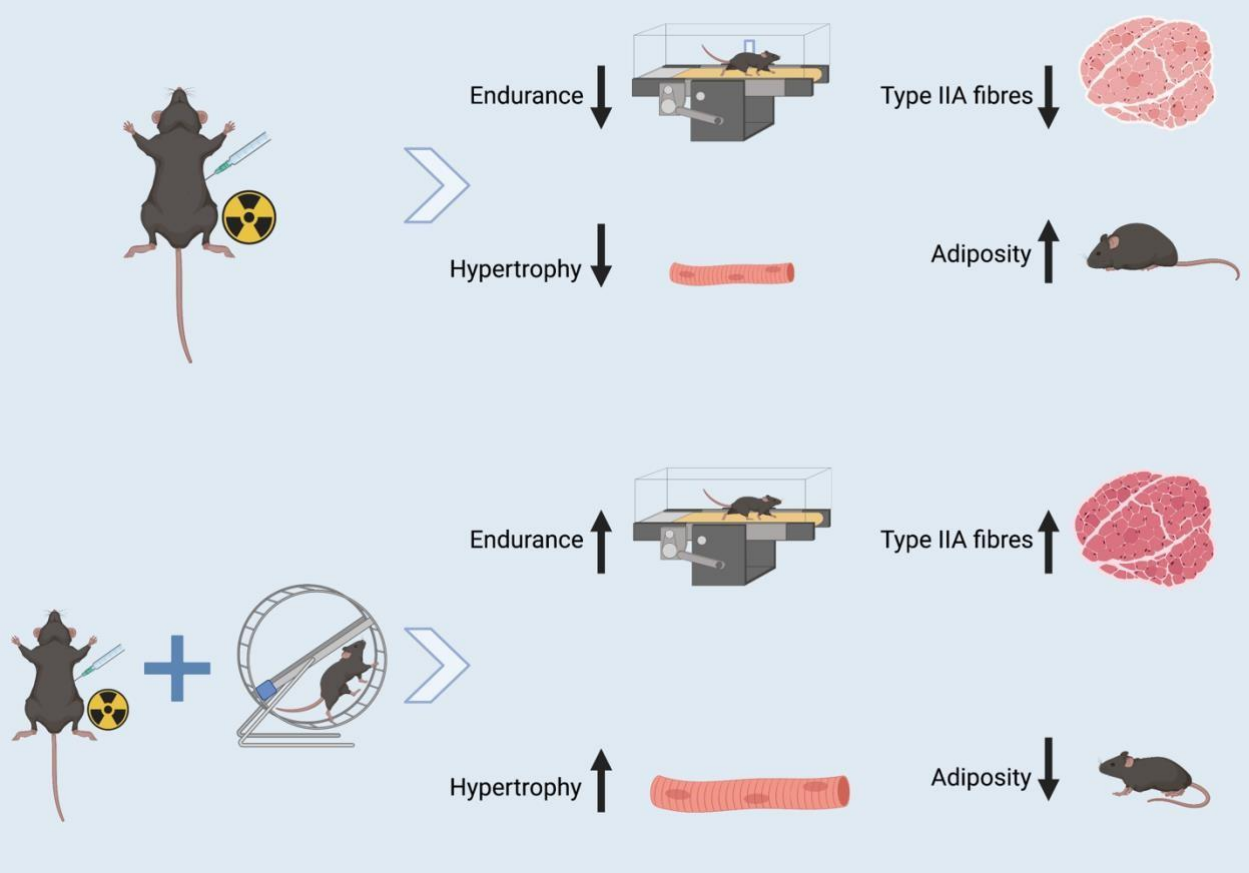

Background: Rhabdomyosarcoma (RMS) is a soft tissue malignancy of the skeletal muscle that occurs primarily in pediatric populations. The prevailing treatment for RMS is a combination of chemoradiation therapy and surgery which has contributed to its 5-year survival rate of 75%. However, the combination of RMS and chemoradiation therapy can lead to impaired muscle growth and development which results in life-long skeletal muscle atrophy and weakness for RMS survivors. Skeletal muscle is a highly plastic tissue due, in part, to dynamic interactions between muscle-resident stem and progenitor cells (i.e., satellite cells (SCs) and fibro/adipogenic progenitors (FAPs)), which

are necessary for muscle maintenance, growth, and adaptation to anabolic stimuli such as resistance exercise training. There is a clear gap in research investigating whether resistance endurance training (RET) stimulates muscle growth and preserves muscle function after juvenile chemoradiation therapy. **Purpose:** To determine the extent to which RET ameliorates the skeletal muscle defects in a preclinical model of RMS survivorship **Hypothesis:** RET will improve physical performance, muscle cross-sectional area (CSA), and stem/progenitor cell populations compared to sedentary mice following RMS and chemoradiation therapy. **Methods:** RMS (M3-9-M cells) was injected into a single hindlimb of juvenile (4 week) C57Bl/6 mice that underwent systemic chemotherapy followed by targeted, fractionated radiation therapy to the RMS-injected limb. Following therapy, mice underwent RET (RET; n=10) or remained sedentary (SED; n=10) for 8 weeks. Body composition and performance tests were completed pre- and post-therapy and throughout the exercise intervention. Fibre typing, cross-sectional area, myonuclear characteristics and trichrome staining were evaluated following muscle harvest and progenitor cell populations were assessed using flow cytometry. **Results:** RET led to increased endurance performance ($p<0.0001$) as well as a reduction in body fat percentage ($p=0.0004$). RET rescued atrophy induced by RMS+therapy as evidenced by a significant increase in gastrocnemius/soleus to body weight ratio for the RET group compared to the SED group ($p=0.0303$), despite the decrease in muscle weight observed in the treated limb compared to the control limb ($p=0.015$). A distinct increase in intramuscular fibrosis was noted in the treated limb compared to the control limb in both groups ($p=0.0283$). Furthermore, RET resulted in larger myofibre cross-sectional area ($p<0.05$) and a shift from Type IIX to IIA fibres ($p<0.05$). We also noted a greater Type IIA myonuclear domain in the RET group compared to the SED group ($p=0.0015$) and an

overall decrease in myonuclear domain (the cytoplasmic volume controlled by each myonucleus) for the treated limb compared to the control limb ($p<0.05$). Interestingly, we noticed overall cell death and an increase in immune cells in the RMS treated limb, while exercise resulted in increased endothelial and mesenchymal stromal cells **Significance:** These preclinical findings will provide the rationale for further investigation of the mechanisms responsible for the beneficial effects of RET as well as optimizing the RET protocol in this juvenile cancer survivorship model.

Chapter I: Literature Review

Introduction

Rhabdomyosarcoma (RMS) is a soft tissue cancer that develops intramuscularly. It is the most common soft-tissue sarcoma found in children, comprising roughly 5% of all childhood cancers (Wasti et al., 2018). RMS primarily affects children younger than 6 years of age (Dagher & Helman, 1999), and has a 5-year survival rate of 75% (Canadian Cancer Society, 2021). RMS is regularly found in the head and neck, GI tract, and extremities. RMS can be further classified into several histological subcategories with embryonal (eRMS) and alveolar (aRMS) being most common; reporting 70% and 25% of all childhood cases respectively (Wasti et al., 2018). Similar to other sarcomas, RMS is considered a micrometastatic disease and is therefore often treated with a combination of radiation and chemotherapy to ensure successful elimination of all tumors and metastases. In fact, prior to a combination of chemoradiation, surgery alone resulted in <20% survival (Dagher & Helman, 1999). Treatment guidelines suggest radiation doses as high as 55-60 Gy to the tumor with Vincristine, actinomycin D, and cyclophosphamide (VAC) chemotherapy. While this treatment regimen has been successful at improving survival, it leads to negative long-term health effects including an increased risk of secondary cancer (Dracham et al., 2018; Kleinerman et al., 1995).

Although the cause of RMS remains ambiguous, it is believed to originate in part from disruptions to skeletal muscle progenitor cell growth and differentiation. Recent work has begun to clarify the mechanisms responsible for aberrant myogenic programming that ultimately leads to RMS (Rossi et al., 2011; Sun et al., 2015; Walters et al., 2014).

Satellite cells (SC) appear to be the cellular origin of RMS when they fail to complete normal differentiation and express unusually high levels of Pax3 (Tiffin et al., 2003). The Myogenic Regulatory Factor (MRF) MyoD plays a critical role in regulating SC differentiation (Cieśla et al., 2014; Sun et al., 2015; M. Zhang et al., 2013). MyoD is also one of the most sensitive markers for identifying RMS (Fiddler et al., 1996); however, in RMS, its normal ability to induce SC differentiation is impaired (Fiddler et al., 1996). It has been postulated that the protein MDM2, a negative regulator of the p53 tumor suppressor, interferes with MyoD activity and this is the cause for inhibited SC differentiation in RMS (Guo et al., 2003). Another contributing factor to the pathogenesis of RMS is the satellite cell microenvironment and extracellular matrix (ECM). Recent work has discovered that RMS leads to increased expression of type XVIII collagen alpha 1 (COL18A1) compared to normal muscle, which has been correlated with worsened survival outcomes (Lian et al., 2021). Fibro-adipogenic progenitors (FAPs), a key multipotent progenitor residing in the SC niche, is well known to lead to intramuscular fibrotic and adipogenic accumulation under pathological conditions and disruption of the ECM when improperly cleared (Joe et al., 2010; Uezumi et al., 2011; Yin et al., 2013). Although imbalance in collagen expression and ECM dysregulation has only recently been discovered as an important factor in RMS development, it has raised the question as to whether FAPs may play a role in the development of RMS through ECM disruption (Lian et al., 2021).

Late Effects of RMS and Chemoradiation on Skeletal Muscle

Considering increased survival rates, the long-term consequences of RMS and its therapies are of emerging and relevant clinical concern. Childhood cancer survivors treated with chemoradiation have an 84% increased risk for chronic health conditions as adults, and a 20% chance of premature death (St. Jude Children's Research Hospital, 2016). It has been proposed that childhood cancer survivors have a physiological phenotype that more closely resembles older adults (i.e., accelerated aging) (Armstrong et al., 2014). It was discovered that survivors over 35 years old were 5 times more likely to develop new onset severe and life-threatening health conditions compared to their age- and sex-matched siblings (Armstrong et al., 2014).

Muscle loss and wasting are side effects of cancer and associated therapies. Not only can this muscular atrophy significantly diminish a patient's quality of life, but there is evidence suggesting that it can limit an individual's ability to endure anti-cancer therapies (Del Fabbro et al., 2012). If the patient survives, muscle loss does not subside and can worsen over time (Hartman et al., 2008; Scheede-Bergdahl & Jagoe, 2013). Several years after vincristine treatment, survivors have significantly reduced peripheral muscular strength (Hartman et al., 2008), as well as decreased exercise tolerance (Hoffman et al., 2013; Jenney et al., 1995). On a fibre-specific level, patients had a significant (>20%) reduction in single muscle fibre CSA (Type I and Type II). This indicates that in other studies which did not find significant hypertrophy using less sensitive whole-body measures, reduced skeletal muscle size is still prevalent on a fibre level (Toth et al., 2016). In fact, there is extensive evidence to support that skeletal muscle dysfunction persists long after cessation of therapy. This is evidenced by a significant reduction in fat-free

mass of childhood leukemia survivors using dual-energy x-ray absorptiometry (Scheede-Bergdahl & Jagoe, 2013). Alterations to skeletal muscle function are particularly important because reduced muscle function is a primary contributing factor to reduced fitness in survivors (Järvelä et al., 2010). Furthermore, a predominant side effect of radiation therapy is radiation-induced fibrosis (RIF) which is the accumulation of fibrotic tissue often accompanied by muscle shortening/atrophy and limited joint mobility (Straub et al., 2015). RIF affects up to 80% of all irradiated cancer patients and is exacerbated in patients that have received chemotherapy (D'Souza et al., 2019; Paulino, 2004; Siegel et al., 2020). Radiation stimulates the excessive proliferation of myofibroblasts causing an overproduction of collagen which is exaggerated by a decrease in extracellular matrix remodeling enzymes (Straub et al., 2015). Moreover, 80% of childhood extremity sarcoma survivors treated with radiation experienced muscle atrophy/ fibrosis and 40% had impaired mobility and extremity function in follow up studies (Paulino, 2004). Together, cancer and its associated therapies can have detrimental effects on quality of life, muscle function, muscle mass, exercise capacity, and leave patients more susceptible to develop additional chronic illnesses later in life (Hartman et al., 2008; Jenney et al., 1995; Scheede-Bergdahl & Jagoe, 2013). These consequences are not simply limited to the acute treatment period and as such, it is necessary to explore interventions that specifically address the long-term muscular dysfunction associated with RMS and therapies.

A recent study that sought to uncover whether chemoradiation would inhibit myofiber hypertrophic growth in a pre-pubertal model of RMS used a novel RMS cell line (M3-9-M) for tumor inoculation (Paris et al., 2020). The authors discovered an additive atrophic effect present in muscle when both chemo and radiation therapy were used in

conjunction as opposed to separately (Paris et al., 2020). They also found that mice exposed to chemoradiation had significant reductions in skeletal muscle function paired with decreases in hypertrophy and cross-sectional area (Paris et al., 2020). Another study with a similar model of local-fractionated radiation took this concept further and addressed some of the immediate and life-long effects of chemoradiation therapy (Bachman et al., 2020). The authors discovered an acute lack of regenerative capacity in skeletal muscle post-radiation (Bachman et al., 2020). Furthermore, the authors showed that well into adulthood mice had life-long deficits in muscle mass, CSA, and regenerative capacity (Bachman et al., 2020).

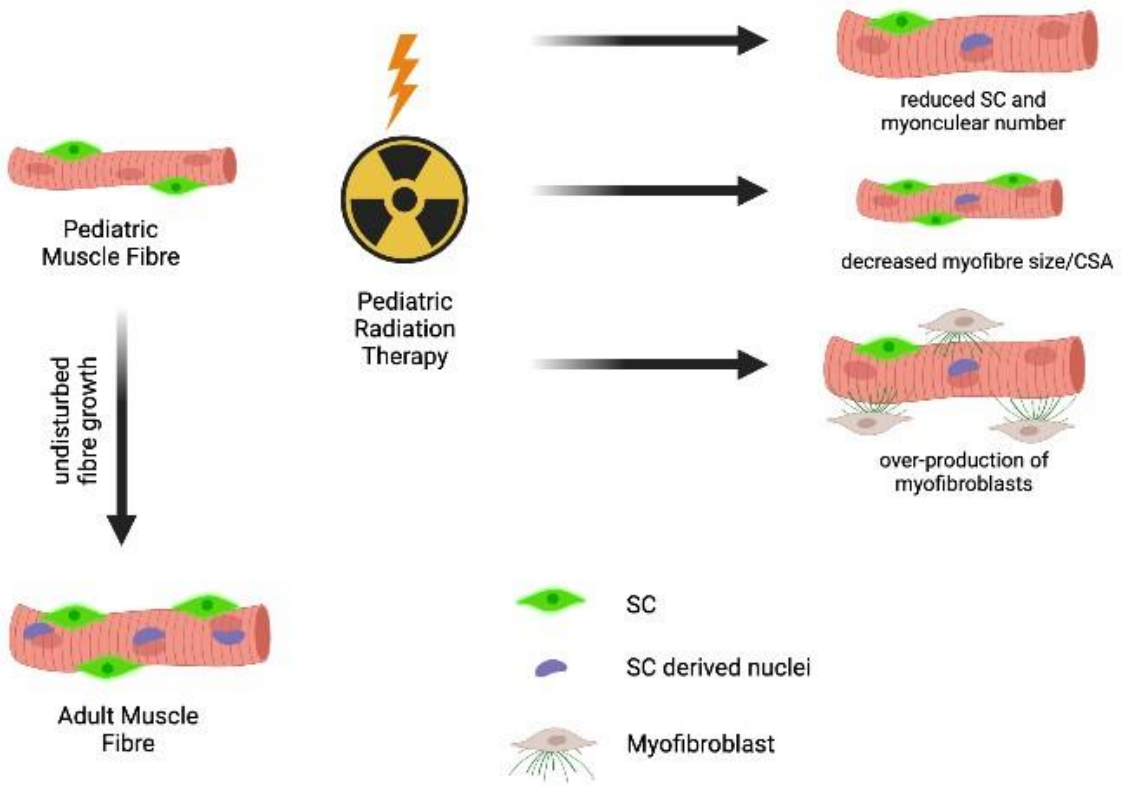

Figure 1. Effects of Pre-pubertal Chemoradiation on Developing Skeletal Muscle

Pediatric chemoradiation can prevent proper myofibre growth and lead to lifelong alterations in skeletal muscle function. These changes are evidenced by persistent decreases in skeletal muscle mass and CSA. Chemoradiation also results in a decrease in SC number and myonuclear number, the mechanism behind reduced muscular regenerative capacity. Finally, an overproduction of myofibroblasts after treatment is a primary contributing factor to increased intramuscular fibrosis and consequentially atrophy and loss of mobility. (Figure created with Biorender).

Muscle Derived Stem and Progenitor Cells in Muscle Regeneration

Skeletal muscle is a highly plastic tissue with the ability to regenerate and repair under conditions of acute and chronic damage. Appropriately functioning skeletal muscle plays a crucial role in proper mobility, metabolism, posture, and activities of daily living (ADL). In the pre-pubertal and early adolescent period, skeletal muscle undergoes an extensive growth period characterized by the expansion of muscle cross-sectional area (CSA) as well as a significant increase in Type II fibres (Lexell et al., 1992). Indeed, disruption to muscular development that occurs during this early stage can have devastating effects on muscle function later in life.

SCs are undifferentiated myogenic stem cells that ultimately result in the production of myofibres. SCs are located between the basal lamina and sarcolemma of muscle fibres and predominantly exist in a quiescent state (Dewys et al., 1980). Their unique ability to contribute new myonuclei and form myofibers during myogenesis makes them an indispensable player in the regulation of skeletal muscle repair and regeneration. The lineage of activated SCs is dichotomous: some differentiate and generate new muscle fibres while others self-renew and maintain the SC pool (Birbrair et al., 2013). The progression of SCs through myogenesis is comprised of five stages: quiescence, activation, proliferation, differentiation, and fusion (Yin et al., 2013). SCs become activated in response to trauma or inflammation (induced in both chronic and acute conditions), proliferate, and then commit to a myogenic fate which results in myoblasts (Seale et al., 2001). SCs are identified by their expression of paired box protein Pax7 (Fu et al., 2015). As they move out of quiescence and into the proliferative phase, SCs begin to express the myogenic regulatory factors MyoD and Myf5 (Fu et al., 2015). Similarly,

MRF4 and myogenin are upregulated during differentiation (Fu et al., 2015). Following muscle damage, myoblasts repair myofibers by migrating to sites of injury using a chemical gradient and fusing their nuclei with the damaged region of the fibre (Seale et al., 2001).

Many studies have established the importance of SCs in skeletal muscle repair (Lepper et al., 2011; Sambasivan et al., 2011). SC depletion demonstrated using fractioned radiation has been shown to reduce SC function, as well as deficits in proliferative and differentiative capacity (Bachman et al., 2018). Furthermore, lingering effects of SC ablation in pre-pubertal muscle lead to life-long deficits in myofiber size and nuclear number, as well as muscle mass (Bachman et al., 2018; Rosenblatt & Parry, 1992). Indeed, numerous other studies have underscored the significance of SCs for their role in preserving physical function and muscle adaptation especially after childhood and throughout development (Bachman et al., 2018; Englund et al., 2020; Scheede-Bergdahl & Jagoe, 2013).

SCs are also required for proper post-natal development and muscular hypertrophy. Contrary to previous literature that assumed SC myonuclear accretion concluded before the prepubertal period, interesting new findings from several groups suggest that residual SC derived myonuclear accretion extends into this period to support myofiber growth (Bachman et al., 2018; Bachman & Chakkalakal, 2021; Cramer et al., 2020; Huh et al., 2017). Studies have discovered that while hypertrophy can occur in a SC depleted *in vivo* model, muscular adaptation and hypertrophy are blunted when compared to a SC replete model (Englund et al., 2021; McCarthy et al., 2011; Murach et al., 2017). Furthermore, SC ablated muscle shows a decrease in muscular force likely due to a decrease in ECM organization to which SCs contribute, as well as increased

fibrosis.

SCs reside in a fluctuating and complex niche that directly impacts how they progress throughout myogenesis. Fibroadipogenic progenitor cells (FAPs), are a population of muscle resident, non-myogenic mesenchymal progenitor cells that are key cellular constituents of the SC niche. They are located between individual myofibres in the interstitial space (Yin et al., 2013), and are identified by their surface marker Platelet Derived Growth Factor Alpha (PDGFRα) (Uezumi et al., 2011). FAPs are unique due to their multipotentency, possessing the capacity to differentiate along osteogenic, adipogenic and fibrogenic lineages (Joe et al., 2010; Uezumi et al., 2011). As a key SC niche constituent, FAPs create a favourable environment for SC activation (Wosczyna & Rando, 2018) and differentiation (Joe et al., 2010), and are catalysts for the successful formation of new muscle fibres by upregulating temporary pro-differentiation signals (Boppart et al., 2013; Joe et al., 2010). Wosczyna and colleagues (2019) specifically ablated FAPs and found a significant reduction in skeletal muscle regenerative capacity as well as increased atrophy, suggesting that FAPs are necessary for muscle regeneration and maintenance. Conversely, in pathological conditions, improper FAP clearance results in their unfavourable accumulation leading to fibro/fatty tissue build-up in muscle (Alves et al., 2017; Collao et al., 2020; Lemos et al., 2015). FAP activation and proliferation are facilitated by proinflammatory cytokines: TNF, IL1, IL13, and TGFβ (Alves et al., 2017; Ueha et al., 2012). The TGFβ pathway creates a fibrotic microenvironment in which unregulated FAP accumulation occurs (Lemos et al., 2015). Accordingly, pathological conditions simulated using *mdx* mice have demonstrated that TGFβ expression from proinflammatory macrophages prevents FAP apoptosis leading to the accretion of fibrotic tissue (Alves et al., 2017; Collao et al., 2020; Lemos et al., 2015).

Moreover, intramuscular fibrotic tissue deposition has been shown to result in impaired muscular function (Collao et al., 2020; Uezumi et al., 2010). In brief, a complex and interconnected balance of cytokines, growth factors, and paracrine signaling is essential for the proper regulation of myogenesis and muscle growth/regeneration.

Effects of RMS and Chemoradiation on the Satellite Cell Niche

Childhood cancers such as RMS occur during the skeletal muscle growth and development stage for which SCs are active and necessary. Notably, activated SCs are more vulnerable to cytotoxic conditions (such as oxidative stress) than those that are quiescent (Pallafacchina et al., 2010; Paris et al., 2020; Scheede-Bergdahl & Jagoe, 2013). Consequently, DNA damage and oxidative stress which are by-products of chemoradiation therapy may be particularly damaging during childhood. They have been shown to impair myoblast proliferation, differentiation, self-renewal, and apoptosis (Y. Chen et al., 2007; Scaramozza et al., 2019).

Indeed, *in vivo* chemotherapy exposure represses MyoD and impairs myogenesis (Paris et al., 2020; Rosenblatt & Parry, 1992). Similarly, SCs are extremely radiosensitive, and the direct effect of oxidative stress caused by irradiation can lead to DNA damage and mutations (Rosenblatt & Parry, 1992). IR has been shown to decrease the proliferative capacity of SCs and attenuate regeneration (Paris et al., 2020; Rosenblatt & Parry, 1992). In fact, Parry and colleagues (1992) discovered that 25 Gy of gamma radiation was sufficient to inhibit SC proliferation and consequently prevented compensatory hypertrophy in a synergistic ablation model. In addition to the direct effects of radiation on SCs, indirect effects related to a sustained systemic inflammatory response

triggered by surviving cells or progeny of cells that had been previously irradiated contribute to prolonged cell damage and tissue dysfunction (Lorimore et al., 2003). Following radiation, several inflammatory cytokines (IL-1b, IL-6, TNFα, TGFβ) that create an inflammatory environment in which SCs and FAPs reside, trigger oxidative stress and lead to tissue damage as well as cell death (Kim et al., 2014). Collectively, both the negative direct and indirect effects on SCs contribute to a pro-inflammatory and degenerative niche in which radiation-induced SC disruption is promoted.

A recent study using the M3-9-M Rhabdomyosarcoma cell line determined that chemoradiation therapy leads to significant reductions in adult muscle myonuclear number and domain due to loss of SC function (Paris et al., 2020). Bachman and colleagues (2020) found an immediate decrease in SC content post-radiation as well as a reduction in proliferation and myogenic commitment. A reduction in myofiber size and loss of nuclei was apparent in radiation induced SC damage. Interestingly, similar results were seen when compared to a previously established model of specific SC ablation ($Pax7^{CreERT2/+;}$ $Rosa26^{DTA/+}$ (P7DTA)) underscoring the necessity of SCs for proper muscle growth (Bachman et al., 2018, 2020). However, a new heterogenous population of reserve SCs ($Mx1^{-}Cre^{+}/Pax3^{+}$), that are radiation resistant, has recently been discovered (Scaramozza et al., 2019). Although regular SCs suffer damage after radiation which reduces their capacity to aid in muscle fibre growth, these special SCs ($Mx1Cre^{+}/Pax3^{+}$) have been shown to minimally aid in muscle regeneration after radiation exposure (Scaramozza et al., 2019). Under specific radiation induced stress they retain the capacity to contribute to muscle repair and SC pool repopulation (Scaramozza et al., 2019). Taken together, this evidence suggests that although necessary for complete treatment of the

tumor, RMS+chemoradiation can inhibit the contribution of SCs to muscle regeneration and hypertrophy.

Effects of Resistance Exercise on Skeletal Muscle

Resistance exercise (relatively low repetitions of muscular contraction performed against external load at a relatively high intensity for a short amount of time) has been shown to diminish muscle wasting in different catabolic situations (Radbruch et al., 2010). Recent studies have underscored the importance of resistance exercise training on preserving muscle mass specifically in cancer survivors (Christensen et al., 2014; Courneya et al., 2007; dos Santos et al., 2019; Kamel et al., 2020). In fact, resistance exercise has been shown to improve muscle strength and fat-free mass in pancreatic cancer-induced cachexia in an older clinical cohort (Kamel et al., 2020). Interestingly, analysis of fibre-specific loss of skeletal muscle mass after chemoradiation discovered that Type I fibres were predominately lost, while Type II fibres were selectively maintained (Toth et al., 2016). This preference to preserve fast twitch fibres may be a way to maintain muscle function in the face of atrophy, and as such these fibres have been posed as an effective target for exercise interventions. However, as a relatively recent field, most resistance exercise studies in cancer survivors have focused on feasibility rather than efficacy. Moreover, few studies focused on skeletal muscle mass as the principal outcome, and of this minority even less were designed with the motive to increase fat-free mass (Courneya et al., 2007; dos Santos et al., 2019; Kamel et al., 2020; Lam et al., 2020). Still, there remains a lack of studies that have assessed resistance exercise following cancer treatment specifically in a pediatric population. Thus, the need to fully

elucidate the mechanisms responsible for hypertrophy after childhood cancer treatment is needed. Many groups have underscored the importance of the niche in moderating the negative effects of aging on tissue regeneration (Cosgrove et al., 2014; Lazure et al., 2021; McKay et al., 2013).

Similarly, endurance exercise has also been shown to contribute to muscle maintenance and specifically improved muscle performance/function and enhanced body composition in cancer survivors (Cave et al., 2018). Childhood cancer survivors, who are uniquely susceptible to cardiovascular disease due to chemoradiation-induced heart damage, have been shown to have increased $V0_2$ max and cardiopulmonary fitness when engaged in aerobic exercise (Bourdon et al., 2018). The most substantiative benefits observed by increased hypertrophy and muscle mass, reduced fat mass, and reduced therapy-induced fatigue were seen in protocols that combined both resistance and endurance training (Segal et al., 2009). In fact, most research that has implemented cardiovascular training in cancer survivors has looked at the cardiorespiratory benefits, while neglecting to assess whole body and muscle composition. While most of the research has been conducted in adult cancer survivors, there is very little information about the efficacy of resistance/endurance training on the juvenile population, and practically no studies that have targeted Rhabdomyosarcoma specifically.

A major limitation to understanding the mechanisms responsible for resistance endurance training induced adaptations in skeletal muscle has been the lack of physiologically relevant animal models. Although there is emerging evidence to support the advantage of exercise in combatting cancer associated muscle dysfunction (Cave et al., 2018; Christensen et al., 2014; Courneya et al., 2007; dos Santos et al., 2019; Kamel et al., 2020), the precise mechanisms behind its effectiveness have yet to be elucidated.

The two most common preclinical models of murine resistance exercise are electrical stimulation and synergistic ablation, with the latter constituting the classical model for studying overload-induced skeletal muscle hypertrophy in rodents (Al-Majid & McCarthy, 2001; Dungan et al., 2019; Otis et al., 2007). Although these methods produce a significant level of hypertrophy within a rather short time frame (>30-50% in 1-2 weeks), they have many drawbacks that hinder their translatability (Khamoui et al., 2016; Lowe & Alway, 2002). These models are invasive, irreversible, and they do not replicate the period required for similar levels of hypertrophy in humans (>6 weeks) (Khamoui et al., 2016). These limitations leave a noticeably large opportunity for an original model of rodent resistance exercise that better reflects the common resistance training in a human population. To address this gap, a recent study conducted by Dungan et al. (2019) demonstrated the effectiveness of a novel mouse resistance/endurance exercise protocol using wheel running. Resistance in the form of magnets placed asymmetrically on a running wheel was increased over an 8-week time frame. This procedure resulted in significant muscular hypertrophy and caused an increase in myonuclear and SC density (Dungan et al., 2019).

This progressive weighted-wheel-running (PoWeR) protocol allowed for the reversibility of training via detraining unobserved in other resistance exercise simulations such as synergistic ablation (Dungan et al., 2019). Moreover, a defining characteristic of this PoWeR protocol was its episodic nature which more accurately reflects human resistance training (Dungan et al., 2019). The mice in this protocol were able to voluntarily engage in short bursts of high-intensity wheel running very similar to daily HIIT (high intensity interval training), a common clinical exercise regimen. Furthermore, PoWeR which is easily modified and has a high degree of flexibility in the amount of resistance

used differs from synergist ablation which is an invasive procedure that cannot be modified after the fact due to its permanent surgical nature (Dungan et al., 2019).

Although other weighted wheel running exercise protocols have been tested, wheel resistance loading was too heavy for the mice to run at a maintainable pace and this ultimately discouraged their sustained exercise (Dungan et al., 2019; Soffe et al., 2016; White et al., 2016). To circumvent this issue, the adjustable resistance facilitated by this new model creates an unequal wheel weight which inherently promotes continued voluntary exercise (Dungan et al., 2019). Another study conducted by the same group has shown that resistance exercise can lead to a strong hypertrophic response in adult skeletal muscle even in an SC depleted condition (Englund et al., 2021). Furthermore, SCs were required for maximal hypertrophy, capillarization, and collagen remodeling in muscle (Englund et al., 2021). There have been no studies that have assessed the effects of resistance/endurance exercise on SC and FAP fate and function specifically after cessation of RMS treatment.

Statement of Problem and Rationale

To summarize the literature presented above: (1) RMS disproportionately affects the pediatric population, (2) childhood RMS and associated therapies result in muscle atrophy and lifelong skeletal muscle deficits, and (3) RET promotes hypertrophy in catabolic and muscle wasting situations such as post-radiation and chemotherapy. It remains unknown; however, the extent to which hybrid resistance/endurance exercise stimulates muscle hypertrophy and adaptations specifically following pre-pubertal chemoradiation. Thus, the purpose of this study is to directly quantify the level of hypertrophy, muscle performance, fat mass/fat-free mass, and fibre-specific adaptations that occurs in developing muscle following RET and chemoradiation in a novel mouse model of Rhabdomyosarcoma. Our overall hypothesis is that RET will improve muscle architecture and function compared to sedentary mice following RMS+therapy. We expect our findings to be significant because it will identify RET as a novel intervention for preventing long-term, late effects of chemoradiation therapy in skeletal muscle of juvenile cancer survivors which will improve their quality of life.

Specific Aims and Hypotheses

To address the above overall objective, we will address the following specific aims:

1) Determine the extent to which RET increases skeletal muscle mass, endurance performance and decreases fat mass post-RMS and chemoradiation therapy
    a. We hypothesize that RET will lead to higher skeletal muscle mass, decreased fat mass, as well as greater grip and endurance strength.
2) Describe the effects of RET on muscle fibre hypertrophy, fibre-specific adaptations, and myonuclear characteristics
    a. We expect larger muscle fibre cross-sectional area, myonuclei per fibre, myonuclear domain and lower fibrosis deposition.
3) Characterize the effects of RET on muscle stem/progenitor cell dynamics following RMS + chemoradiation therapy.
    a. We hypothesize that RET will lead to higher SC and FAP content following RMS treatment

Chapter II: Research Article

Resistance endurance training improves muscle mass and the inflammatory/fibrotic transcriptome in a rhabdomyosarcoma model

Olivia Sanders1†, Nicolas Collao1†, Taylor Caminiti1, Laura Messeiller1, and Michael De Lisio1,2*

1School of Human Kinetics, and 2 Department of Cellular and Molecular Medicine, Regenerative Medicine Program, University of Ottawa, Ottawa, ON, Canada
†These authors contribute equal to this work.

Keywords: Fibrosis, Radiation, Chemotherapy, Muscle Satellite cells, Fibro-adipogenic progenitors, Inflammation, Cachexia, Exercise, Cancer

***Corresponding author information:** Michael De Lisio, School of Human Kinetics, and Department of Cellular and Molecular Medicine, Regenerative Medicine Program, University of Ottawa, Ottawa, ON, Canada. Phone: +1 613-562-5800 ext. 6987. Email: mdelisio@uottawa.ca

Abstract

Background: Rhabdomyosarcoma (RMS) is an aggressive soft tissue sarcoma that most often develops in children. Chemoradiation therapy is a standard treatment modality; however, the detrimental long-term skeletal muscle consequences of these therapies in juvenile cancer survivors include muscle atrophy and fibrosis resulting in decreased physical performance. Using a novel model of murine resistance endurance training, we investigate its role in preventing the long-term effects of juvenile RMS plus therapy.

Methods: Four-week-old Male (n=10) and Female (n=10) C57BL/6J mice were injected with M39-M RMS cell into the left gastrocnemius (GAS) with the right limb serving as an internal control (CON). Mice received a systemic vincristine injection, and then five doses of 4.8 Gy of gamma radiation localized to the left hindlimb (RMS+Tx). Mice were then randomly divided into either sedentary (SED) or resistance endurance-trained (RET) groups which were house without a wheel or maintained and 8-week wheel running protocol of increasing weight respectively. Changes in exercise performance, body composition, myocellular adaptations, and inflammatory/fibrotic gene profile were assessed.

Results: RET improved endurance performance ($p<0.0001$) and body composition ($p=0.0004$) compared to SED. RMS+Tx resulted in significantly lower muscle weight ($p=0.015$), and significantly smaller myofibre cross-sectional area (CSA) ($p=0.014$). Conversely, RET resulted in significantly higher muscle weight ($p=0.030$) and significantly larger Type IIA ($p=0.014$) and IIB ($p=0.015$) fibre CSA. RMS+Tx resulted in significantly more muscle fibrosis ($p=0.028$) which was not reversed by RET. RMS+Tx resulted in significantly fewer mononuclear cells ($p<0.05$) and muscle satellite (stem) cells (MuSCs)

(p<0.05), and significantly more immune cells (p<0.05) compared to CON. RET resulted in significantly more fibro-adipogenic progenitors (FAPs) (p<0.05), a trend for more MuSCs (p=0.076) compared to SED, and significantly more endothelial cells specifically in the RMS+Tx limb. Transcriptomic changes revealed significantly higher expression of inflammatory and fibrotic genes in RMS+Tx, which was reversed by RET. In the RMS+Tx model, RET also significantly altered expression of genes involved in the hypertrophic mTOR pathway, and extracellular matrix (ECM) turnover.

Conclusions: Our study suggests that RET preserves muscle mass and performance in a model of juvenile RMS survivorship by increasing hypertrophic signaling and reducing inflammatory signaling.

Introduction

Rhabdomyosarcoma (RMS) is an intramuscular cancer and is the most common soft tissue sarcoma found in children, comprising roughly 5% of all childhood cancers (Wasti et al., 2018). RMS is considered a metastatic disease and is therefore often treated with a combination of radiation and chemotherapy (Chen et al., 2019). While chemoradiation has successfully improved survival rates as high as 70-90% for the most common low-grade tumours, it leads to adverse long-term, late effects such as muscle atrophy and fibrosis in approximately 80% of juvenile sarcoma survivors (De Ruysscher et al., 2019; Paulino, 2004). Preclinical models have begun to elucidate the mechanisms responsible for these effects which include reduction of muscle stem (satellite) cell (MuSC) content (Bachman et al., 2020; Paris et al., 2020), increased expression of fibrotic genes, and inflammation (Kallenbach et al., 2022). As a result, juvenile sarcoma survivors experience a high prevalence of muscle weakness (Hartman et al., 2008), fatigue, exercise intolerance (Gilliam & St Clair, 2011), morbidity, and disability (Stubblefield, 2011). These negative consequences are particularly prevalent in juvenile survivors due to their longer lifespan after therapy, and exposure to these toxic therapies occurring during skeletal muscle growth and development (Paulino, 2004). As such, there exists a critical need for novel interventions to prevent the long-term late effects of cancer plus therapy in skeletal muscle of juvenile cancer survivors.

Pre-pubertal skeletal muscle development and growth depends on a functioning population of MuSCs (Bachman et al., 2018). MuSCs are quiescent myogenic cells, located in the periphery of the muscle fibre between the sarcolemma and the basal lamina (Mauro, 1961) and commonly identified by the expression of the transcription factor paired

box protein, Pax7 (Yin et al., 2013). Following muscle injury, MuSCs rapidly activate and enter the cell cycle, proliferate, and differentiate to regenerate the muscle tissue; while a small fraction returns to quiescence to replenish the MuSC pool to support future regeneration (Yin et al., 2013). Paris and colleagues (2020) demonstrated that juvenile RMS plus therapy depletes MuSCs and impairs normal muscle growth. MuSC depletion by cancer therapy was particularly damaging to muscle mass in juvenile mice compared to adult mice (Bachman et al., 2020), further supporting the importance of exposure to cancer and its associated therapies prepuberty. Proper MuSC regulation requires a functioning niche consisting of vascular endothelial cells (ECs), immune cells, and fibro-adipogenic progenitors (FAPs) (Mashinchian et al., 2018; Sousa-Victor et al., 2022). Cancer therapy is known to deplete endothelial cells in several tissues (Williams et al., 2016) and alters immune cell phenotype and function in skeletal muscle which contributes to impaired muscle regeneration (Patsalos et al., 2017). The effects of cancer therapy on FAPs have received relatively less attention; however, early evidence suggests that cancer therapy does not impact FAP content in mice (Kallenbach et al., 2022). Further, gene expression analysis revealed that cancer therapy creates a pro-inflammatory environment and an aberrant ECM deposition which persist long-term after exposure in a preclinical model (Straub et al., 2015). As such, interventions to prevent deleterious alterations to niche mediated MuSC dysfunction in juvenile cancer survivors may improve long-term outcomes.

Endurance and resistance exercise training are recommended for cancer survivors as an effective non-pharmacological strategy that improves muscle strength and endurance

performance resulting in improved quality of life for cancer survivors (Campbell et al., 2019). These recommendations are derived primarily from adult survivors of breast, prostate, and colorectal cancer with no specific recommendations for juvenile cancer survivors (Braam et al., 2016). Exercise training in cancer survivors can improve body composition, although to a lesser degree than in healthy adults (Clifford et al., 2021) and induces muscle growth (Koeppel et al., 2021). Mechanistically, endurance exercise training enhances skeletal muscle antioxidant and mitochondrial enzyme activity following radiation exposure (De Lisio et al., 2011). These alterations to enzyme activity likely underlie the recently revealed reduction in markers of radiation-induced damage, mitochondrial reactive oxygen species production, and improved maintenance of muscle mass in physically active mice (O'Connor et al., 2022). Further, recent work from our lab suggests that endurance exercise training before and after radiation therapy can increase MuSC and FAP content in post-pubertal mice (D'Souza et al., 2019). Whether exercise training can improve long-term, skeletal muscle late effects in a preclinical model of juvenile RMS plus therapy survival remains unknown.

In healthy muscle, eccentric exercise facilitates MuSCs mobilization, and studies have demonstrated that MuSCs exert a powerful influence in the adaptative muscle response (Valero et al., 2012; Zou et al., 2015). Furthermore, both resistance training and endurance training have been shown to reduce pro-inflammatory and enhance anti-inflammatory pathways; specifically, a reduction in IL-6 and IL-1β and enhancement of IL-1ra responses (Ihalainen et al., 2017), as well as decreased C-reactive protein (Mattusch et al., 2000). Additionally, several signaling factors released during resistance exercise inhibit FAP adipogenesis proposing a mechanism whereby acute muscular damage can prevent intermuscular adipose accretion under metabolic stress (De Lisio et al., 2014;

Farup et al., 2015). It remains unknown; however, the extent to which combined resistance and endurance training can prevent the long-term effects of juvenile cancer plus therapy.

Preclinical interventions that model combined endurance and resistance exercise training have been wanting due to a lack of translational models of murine resistance exercise. Recent work, using a model of resistance endurance training (RET) that uses an unbalanced weight applied to a running wheel has been shown to induce MuSC expansion and MuSC-mediated muscle hypertrophy in young and aged mice (Dungan et al., 2019; Englund et al., 2021). To begin to elucidate the mechanisms responsible for RET-induced improvements in skeletal muscle in cancer survivors, we combine these newly established models of juvenile RMS plus therapy (Paris et al., 2020), and progressive RET (Dungan et al., 2019), to examine the extent to which RET improves body composition, exercise performance, myocellular characteristics, and inflammatory/fibrotic gene expression in skeletal muscle. We hypothesized that RET would prevent several of the skeletal muscle defects induced by juvenile RMS plus therapy by improving cellular components and gene expression of soluble factors in the MuSC niche.

Methods

Ethics statement, mice, and experimental design

Ethical approval for this project was obtained from the University of Ottawa Animal Care and Veterinary Service Committee and performed according to the Canadian Council on Animal Care's guidelines. Mice were housed under specific pathogen-free conditions in a controlled facility (temperature 22-25 °C, 30% humidity and 12-hour light: dark cycle) with food and water provided *ad libitum*. Four-week-old male (n=10) and female (n=10) C57BL/6 mice were purchased from The Jackson Laboratory (Bar Harbor, ME) and were allowed to acclimatize to the animal facility for one week prior to use in any experiments. All mice received RMS injections into the left hindlimb followed by systemic chemotherapy and localized, fractionated radiation to the RMS-injected limb. Following RMS+therapy (RMS+Tx) mice were equally divided into either a sedentary (SED) or RET group (Figure 1A).

Rhabdomyosarcoma + therapy model

The RMS+Tx model was conducted as previously described (Paris et al., 2020). The M3-9-M RMS cell line (a kind gift from Dr. Crystal MacKall, Stanford University) was established by harvesting a tumor residing in the HGFTg+p53+/- mouse, then embedding whole tumor fragments into the leg of a C57BL/6 recipient and collecting metastatic tumors from intraabdominal lymph nodes (Meadors et al., 2011). This specific model of cancer was chosen because RMS is a common childhood cancer, the M3-9-M cell line is syngeneic with C57BL/6 mice, it can be injected intramuscularly, and localized to the

muscle of interest for targeted radiation therapy. M3-9-M cells were cultured in RPMI media 1640 (Cat# 350-000-CL, Wisent Inc) containing 1% Lglutamine (Cat# 07100; StemCell Technologies), 10% heat-inactivated fetal bovine serum (Cat# 12483-020; Gibco), HEPES (Cat# 15630-080, Gibco), 1% non-essential amino acids (Cat# 11140050, Gibco), 1% sodium pyruvate (Cat# 11360-070, Gibco), 1% penicillin/streptomycin (P/S) (Cat# 15140-122, Thermo Fisher Scientific), and 50 mM 2-mercaptoethanol (Cat# 21985-023, Gibco) (Meadors et al., 2011).

For tumor inoculation, all mice were sedated using isoflurane and fur was removed via clippers from each hindlimb. 100,000 M3-9-M cells were resuspended in sterile PBS and injected into the left GAS of each mouse using an insulin syringe in two injections into each lobe of the GAS (Meadors et al., 2011). The right GAS was injected in the same manner with sterile PBS. Mice were left to recover without manipulation for three days post-tumor injection. Tumor progression was monitored daily using gross-examination and palpation, and health checks were recorded for 3-days post injection. On day four after RMS injection, each mouse received a dose (1 mg/kg per body weight) of the systemic chemotherapeutic agent vincristine sulfate (Cat#V8388, Sigma Aldrich) diluted in sterile PBS via intraperitoneal (IP) as previously described (Paris et al., 2020). All four-week-old C57BL/6 mice were first weighed to ensure they were ≥ 12 g before vincristine treatment to minimize risk of mortality or illness that accompany the medication's toxicity (Paris et al., 2020). Mice were housed in sterile cages and received antibiotic (Baytril) water *ad libitum* for one week to decrease the risk of infection. At five weeks of age, all mice were exposed to fractioned radiation of five doses of 4.8 Gy localized to the RMS-injected limb (Monday to Friday) (X-RAD 320, Precision X-Ray Irradiation) as previously described (Paris et al., 2020). The rest of the body was protected using a lead murine

abdomen shield and the contralateral non-RMS-injected, non-irradiated limb was used as an internal control (CON). Mice were anaesthetized with isoflurane via a nose cone and maintained under anesthetic during all radiation procedures. This sublethal radiation schedule has a BED (biologically effective dose) score on the lower end of the clinical range yet has been shown to successfully eliminate RMS tumors in juvenile C57BL/6 mice (Paris et al., 2020). Post-radiation therapy, mice were transferred to sterile cages as to prevent infection and monitored daily.

Four mice perished after cessation of therapy, and recurrence of tumors were detected upon resection in three mice, therefore a total of 16 mice for both RET (n=7) and SED (n=9) groups were used in analysis of anthropometric measures. Of all muscle excised, muscles for six mice in the RET group (n=6) and eight in the SED group (n=8) were of sufficient quality to use for myonuclear and myosin heavy chain staining.

Resistance endurance training (RET)

At six weeks of age, mice were randomly assigned into either a RET (n=10) or SED (n=10) groups. RET was conducted as previously described (Dungan et al., 2019). Mice in the RET group were housed with weighted running wheels while mice in the SED group were housed with no wheel for 8 weeks (Dungan et al., 2019). After one week of wheel acclimatization with no weight (week 0), RET began with a resistance of 2 g in week 1 and this weight was increased gradually by 1 g/week until a weight of 5 g was maintained for 2 weeks (weeks 4-5) and then increased to 6 g which was maintained for the final 3 weeks (weeks 6-8). Wheels were loaded on their periphery with 1 g magnets (K&J Magnetics), fastened in a single uniform location on the circumference of the wheel, thus creating an imbalanced load which the mice had to overcome with each revolution

(Dungan et al., 2019). Progressive overload was facilitated by increasing weight over time (Dungan et al., 2019). Running speed (km/h), distance (km/day), and time (h/day) were tracked daily using low profile wireless running wheels (ENV-044, ENV-047, Med Associates) and associated software packages (Wheel Manager Software SOF-860, Wheel Manager Data Analysis Software SOF-861, Med Associates)

Endurance Testing

Endurance performance was evaluated at baseline (Pre-Tx), after chemoradiation treatment (Pre-RET), and after the RET intervention (Post-RET) as previously described (Farber et al., 2021). Prior to endurance testing, mice were acclimatized to the testing room for 30 minutes and then placed in individual lanes on a motorized treadmill (Columbus Instruments). Testing began at a speed of 11 m/min which was increased by 1 m/min every 2 minutes until a mouse met one of the following three criteria to end the test: 1) resisted stimulation with rubberized tweezers, 2) remained stationary on the treadmill platform off of the belt for greater than 2 minutes, or 3) remained one body length away from the platform for greater than 5 seconds and could not increase speed when stimulated (Farber et al., 2021). Electric shock was not used in this study. The time and speed at which each mouse reached volitional exhaustion was recorded by investigators blinded to experimental group.

Grip Strength Testing

Maximal grip strength for both fore- hindlimbs combined was measured as previously described (Farber et al., 2021; Zou et al., 2015). Mice were tested prior to endurance testing at Pre-Tx, Pre-RET, and Post-RET using the Chantillion DFE II (Columbus Instruments). Briefly, mice were acclimatized to the testing room for 30 minutes then placed on the force gauge grid gripping station and allowed to rest for a few seconds to ensure all 4 limbs were gripping the grid. Mice were gently but quickly pulled straight backwards, horizontally off the grid at a consistent speed. A total of five grip strength tests were performed on each mouse. The highest and lowest force values were discarded and an average of the remaining three values were used to score each mouse. The test was implemented by the same investigator on each mouse to minimize variability and the investigator was blinded pre-analysis to experimental groups.

Body Composition Measurements

Body composition and body weight was assessed at Pre-Tx, Pre-RET, and Post-RET using the EchoMRI-900 (EchoMRI LLC) and an electronic scale as previously described (Emmons et al., 2019; Farber et al., 2021)**.**

Tissue collection

GAS were carefully dissected 3 days after the last bout of exercise and used for total weight, CSA, myosin heavy chain, myonuclear domain, flow cytometry, and gene expression analyses. Muscles were either embedded in tissue-embedding medium (OCT, Cat# 4585, Fisher Scientific) prior to freezing in liquid nitrogen-cooled isopentane (Cat#

277258-1L, Sigma-Aldrich), flash frozen for Nanostring analysis, or weighed for immediate processing to be used in flow cytometry analysis. Frozen samples were preserved at -80^{o}C prior to analysis.

Histochemical, immunostaining, and microscopy

Transverse sections of GAS were taken from the mid-belly at 10 µm thickness using a HM 525 NX-2210 cryostat (Leica, Wezlar, Germany) and placed onto glass slides (Cat# 12-544-2, Fisher Scientific). An average of 482 ± 22.5 muscle fibres per mouse were analyzed for CSA, fibre type proportion, and myonuclear domain. The Histology Core and the University of Ottawa conducted the Masson's Trichrome staining and analysis was conducted as previously described. Myosin Heavy Chain (MyHC) staining was conducted as previously described (Dyar et al., 2014), for fibre-type specific CSA, fibre-type distribution, and myonuclear density. Briefly, muscle sections were incubated in a cocktail of isotype-specific anti-mouse primary antibodies: MyHC-I, IgG-2b (1:100, Cat# BA-D5, DSHB), MyHC-IIA, IgG1 (1:100, Cat# SC-71, DSHB), MyHC-IIB, IgM (1:25, Cat# BF-F3, DSHB), and anti-laminin (IgG, 1:50, Cat # MA1-06100 Monoclonal Antibody (A5), Thermo Fisher Scientific). Sections were then incubated in the corresponding secondary antibodies to selectively bind each primary antibody: Alexa Fluor® 647 AffiniPure Goat AntiMouse IgG, Fcγ subclass 2b specific (1:100, Cat# 115-605-207, Cedarlane Laboratories), Alexa Fluor® 488 AffiniPure Goat Anti-Mouse IgG, Fcγ subclass 1 specific (1:100, Cat# 115-545-205, Cedarlane Laboratories), Cy™3 AffiniPure Fab Fragment Goat Anti-Mouse IgM, µ chain specific (1:50, Cat# 115-167-020, Cedarlane Laboratories), and Alexa Fluor 594 (Cat # A11005, Invitrogen) used for detection of Laminin. Type IIX fibres were identified as unstained for MyHC I, IIA, or IIB. Hybrid fibres

were identified as those staining for more than 1 MyHC isoform. Myonuclei were identified as nuclei with at least 50% of their area beneath the basal lamina. Myonuclear domain was calculated by dividing the average number of myonuclei by the average CSA (μm^2) per sample. Images for Masson's Trichrome staining were acquired using an EVOS-FL2 Automated Microscope (Thermo Fisher Scientific), while a ZEISS CellDiscoverer7 (ZEISS) automated microscope was used to capture fluorescent images. Brightness and color contrast was adjusted, and images analyzed using ImageJ software by a blinded investigator.

Flow cytometry

Skeletal muscle preparation for flow cytometry analysis was performed as previously described (Feige & Rudnicki, 2020). Briefly, GAS were carefully dissected, and connective tissue and fat were removed. Muscles were washed with cold-PBS and transferred to a Miltenyi GentleMACS C tube (Cat# 130-093-237, Miltenyi Biotec) containing Collagenase B (1.5U/ml, Cat# 11088831001; Sigma-Aldrich) and Dispase II, (2U/ml, Cat# 42613-33-2; Sigma Aldrich) in Ham's F10 media (Cat# 318-050-CL, Wisent Inc) by gentleMACS Octo Dissociator (Cat# 130-096-427, Miltenyi Biotec) then passed through a 100 µm strainer (Cat# 22-363-549, Fisher Scientific) followed by centrifugation at 600 x *g* at 4°C for 10 min. The pellet was resuspended in Red Blood Cell Lysing Buffer (Cat# R7767; Sigma-Aldrich) and centrifuged. The pellet was resuspended in ice-cold flow buffer (10% FBS, 3 mM of EDTA in 1xPBS) and the cell preparation was incubated with primary antibodies against CD45 (FITC Rat Anti-Mouse CD45, Cat# 561088, BD Biosciences), CD31 (BV510 Rat Anti-Mouse CD31, Cat# 563089, BD Biosciences), ITGA7 (anti-Alpha 7 Integrin 647, Cat# 67-0010-05, AbLab), and Ly-6A/E (Sca1) (BV711

Rat Anti-Mouse Ly-6A/E, Cat# 563992, BD Biosciences) at 4°C in the dark for 35 minutes then washed prior to analysis. For all antibodies, fluorescence minus one (FMO) and single-stained controls were used to established gates and compensation. Cell viability was assessed with SYTOX™ green (Cat# S34860, Invitrogen). Hematopoietic cells were identified as $CD31^{-}/CD45^{+}$. Endothelial cells were identified as $CD45/CD31^{+}$, MuSCs were identified as $CD45^{-}/CD31^{-}/Sca1^{-}/ITGA7^{+}$ and Fibro-adipogenic progenitors were identified as $CD45^{-}/CD31^{-}/ITGA7^{-}/Sca1^{+}$. Flow cytometric analysis was performed using a NxT flow cytometer and processed in FlowJo™ v10.8 Software (BD Life Sciences). Analyses were conducted by an investigator blinded to experimental group.

Nanostring nCounter assay and data analysis

Total RNA isolation from GAS was performed using MicroKit (Cat# 74004, Qiagen) according to manufacturer's instructions. RNA purity and concentration were measured with a Nanodrop 2000c spectrophotometer (Thermo Fisher Scientific). Targeted transcriptomic analysis of a specific CodeSet panel of genes involved in muscle fibrosis and inflammation was performed with a Nanostring nCounter Mouse Fibrosis V2 panel (Cat# 115000388, NanoString Technologies). This panel allows for the investigation of 770 genes across 51 annotated pathways. Samples (100 ng of RNA) were prepared and analyzed on the multiplexed digital nCounter® platform (NanoString Technologies) according to the manufacturer's instructions. Briefly, all samples were hybridized to a reporter that was specific to the target gene and capture probes in a thermocycler overnight at 65°C. Samples were added to the nCounter cartridge and loaded into the multiplexed digital nCounter® platform. Reporter code counts (RCC) and reporter library file (RFL) were generated, and quality control, background subtraction, and normalization

were performed using the nSolver 4.0 Software (NanoString Technologies). Normalized RCC files were analyzed using ROSALIND® nCounter Data Analysis Software (https://rosalind.bio/), with a HyperScale architecture developed by OnRamp BioInformatics, Inc. During the quality control process, a multidimensional scaling (MDS) plot was generated. The cell type profiling module calculates the abundance of various cell populations. Using the fast method, described in nCounter Advanced Analysis (MAN-10030-03) fold-changes and p-values were calculated. The Benjamini-Hochberg method of estimating false discovery rates (FDR) was used for the adjusted p-value. Genes clusters for heatmaps of differentially expressed genes (DEGs) were performed using the PAM (Partitioning Around Medoids) method using the fpc R library (*Hennig, C. CranPackage Fpc. Https://Cran.Rproject.Org/Web/Packages/Fpc/Index.Html*, n.d.). Hypergeometric distribution was performed to analyze the enrichment of pathways, gene ontology (GO), and other ontologies. The topGO R library (*Alexa A, Rahnenfuhrer J. TopGO: Enrichment Analysis for Gene Ontology. R Package Version 1.38.1 (2019)*, n.d.) was used to determine local similarities and dependencies between GO terms.

Statistical analyses

Data are expressed as mean ± standard error of the mean (SEM). A p value ≤ 0.05 was considered statistically significant. The number of biological replicates (n) for each experiment are indicated in the figure legend. A three-way mixed analysis (time x group x treatment) of variance assessed differences between the whole-body outcomes (i.e., body composition, body weight), and functional outcomes (i.e., grip strength and endurance). A two-way mixed analysis (treatment x group) of variance assessed differences in muscle architecture (i.e., fibre specific cross-sectional area, fibre type proportions, fibrosis) myonuclear characteristics (i.e., fibre type specific myonuclei per fibre and myonuclear domain), and flow cytometry analysis. Sidak posthoc tests were used to determine differences if interaction effects were present and to control for family wise error rate. Statistics and graphs were prepared using GraphPad Prism version 8.0.1 software (GraphPad Software)

Results

Resistance endurance training improves endurance performance and body composition post-RMS plus therapy

Mice in the RET group ran approximately 5.86 ± 0.44 km per day which was consistent across the 8-week intervention. This intermittent daily exercise can be best translated to low intensity/high volume interval training modality seen in humans (Figure 1B). There was no significant effect of RMS+Tx on endurance performance; however, RET had higher endurance performance compared to SED at Post-RET (Figure 1C, $p<0.0001$). Grip strength significantly increased at Pre-RET compared to Pre-Tx, and further increased at Post-RET with no differences between SED and RET (Figure 1D, $p=0.300$). There was a significant increase in body weight over time in Month 1-RET compared to baseline, Pre-Tx, and Start-RET; Month 2-RET compared to baseline, Pre-Tx, Start-RET, and Month 1-RET; End-RET compared to baseline, Pre-Tx, Start-RET, Month 1-RET, and Month 2-RET; Endpoint compared to baseline, Pre-Tx, Start-RET, Month 1-RET, and Month 2-RET (Figure 1E, $p<0.0001$). No differences in body weight between SED and RET were observed at any timepoints (Figure 1E). RET had significantly less body fat percentage than SED at Post-RET (Figure 1F, $p=0.0004$). Although no differences in lean mass between experimental groups exist, significantly greater lean mass was recorded between Pre-RET and Pre-Tx timepoints, as well as between Post-RET and Pre-RET and Pre-Tx timepoints for all mice (Figure 1 G, $p<0.0001$).

RMS plus therapy led to muscle atrophy and fibrosis

GAS weight was significantly lower in RMS+Tx compared to CON (Figure 2A, $p<0.05$) and was significantly higher in RET versus SED (Figure 2A, $p<0.05$). Significantly more extracellular matrix accumulated in the RMS+Tx limb versus the CON limb with no effect of RET ($p=0.028$, Figure 2C). Representative Masson's trichrome images depicting all four conditions (CON-SED, CON-RET, RMS+Tx-SED, and RMS+Tx-RET) are presented in Figure 2C.

Resistance endurance training increased myofibre CSA and induced alterations in fibre type distribution independent of RMS plus therapy

Representative myosin heavy chain (MyHC) images of GAS are presented in Figure 3A. MyHC Type I and hybrid fibres were inconsistently detected across samples, thus were excluded from final analyses. Total fibre CSA was significantly larger in RET compared to SED (Figure 3B, $p=0.0087$). The SED group had significantly more 2000-2400 μm^2 fibres than the RET group in the CON limb (Figure 3C, $p=0.011$), and a trend for more fibres <400 μm^2 was detected in the SED versus the RET group in the RMS+Tx limb (Figure 3D, $p=0.065$). Type IIA Myofibre CSA was not changed with RMS+Tx but was significantly larger in RET compared to SED mice (Figure 3E, $p=0.014$) Type IIB CSA was significantly smaller in the RMS+Tx limb versus the CON limb (Figure 3F, $p=0.006$) and was significantly larger in RET versus SED (Figure 3F, $p=0.015$). Type IIX CSA was not altered by RMS+Tx but displayed a trend for larger CSA in RET versus SED (Figure 3G, $p=0.059$). The proportion of Type IIA fibres was significantly higher in the RMS+Tx limb compared to the CON limb (Figure 3H, $p=0.004$), and was also higher in RET versus SED mice (Figure 3H, $p=0.025$). Correspondingly fewer Type IIB fibres were observed in the RMS+Tx limb versus the CON limb (Figure 3I, $p=0.006$) as well as in RET versus SED

mice (Figure 3I, p=0.025). No significant differences in Type IIX fibre proportion were observed with RMS+Tx or RET (Figure 3J).

Increase in myonuclear domain with no changes in myonuclear accretion followed RMS plus therapy and resistance endurance training

Representative myonuclear and laminin staining is presented in Figure 3A. Total myonuclear domain, the cytoplasmic volume controlled by each myonucleus, was significantly larger in the CON-RET versus RMS+Tx-RET (Figure 4B, p<0.001), and a trend for larger myonuclear domain in CON-RET versus CON-SED was observed (Figure 4B, p=0.090). Type IIA fibre myonuclear domain was significantly larger in RET versus SED (Figure 4C, p=0.001). A larger domain was observed in Type IIB fibres in CON-RET versus CONSED (p=0.013) and RMS+Tx-RET (p=<0.001) (Figure 4D). A trend for greater myonuclear domain size was also observed in RET versus SED for Type IIX fibres (Figure 4E, p=0.086). No differences in nuclei per fibre were observed in all fibre types combined, or Type IIA, Type IIB, and Type IIX fibres independently (Figure 3 F-I).

RMS plus therapy and resistance endurance training induce changes in cellular dynamic in skeletal muscle

Representative flow plots for various skeletal muscle mononuclear cell populations are presented in Figure 5A. Total live, mononuclear cell count per muscle weight was significantly lower in the RMS+Tx limb compared to the CON limb (Figure 5B, p<0.05). The RMS+Tx limb had a higher number and proportion of $CD45^+$ cells compared the CON limb (Figure 5C-D, p<0.05), while a trend for more $CD45^+$ cells was observed in RET versus SED mice (Figure 5C, p=0.065). A greater number of $CD31^+$ cells in RET compared to SED mice was observed in the RMS+Tx limb (Figure 5E, p<0.05) and there was a trend for fewer $CD31^+$ cells in RMS+Tx-SED compared to CON-SED (Figure 5E,

p=0.093). RET had a higher proportion of $CD31^+$ cells compared to SED (Figure 5F, p<0.05). The RMS+Tx limb had fewer $\alpha7^+$ cells compared to the CON limb (Figure 5G, p<0.05), while RET had a trend for more $\alpha7^+$ cells compared to SED (Figure 5G, p=0.076). There was no significant effect of RMS+Tx or RET on $\alpha7^+$ cell proportion (Figure 5H). RET had more $Sca1^+$ cells per muscle weight (Figure 5I, p=0.022). There was a trend for fewer $Sca1^+$ cells in RMS+TX-SED compared to CON-SED (Figure 5I, p=0.068). A higher proportion of $Sca1^+$ cells was observed in RET compared to SED mice (Figure J, p<0.05).

Fibrotic and inflammatory signature is induced by RMS plus therapy and is partially reduced by resistance endurance training in skeletal muscle

The multidimensional scaling (MDS) plot shows transcriptional expression distinguishes CON and RMS+Tx groups independent of RET/SED condition (Figure 6A). Cell Profiler indicates an enrichment of Mast cells, Macrophages and CD45 cells in RMS+Tx compared to CON (Figure 6B). A volcano plot showing the differentially expressed genes (DEGs) up-regulated (log_2 fold change > +0.5) and down-regulated (log_2 fold change < -0.5) between the CON-RET vs CON-SED groups (Figure 6C, p<0.05). Eight genes (*Cd36, Cxcr4, Gbp3, Oasl1, Tnfsf10, Mmp12 and Angptl4*) were upregulated and four genes were down-regulated (*Lep, Adipoq, Irf4* and *S100a4)* in the CON-RET compared with CON-SED group. The Top 10 gene set analysis (GSA) performed for this specific fibrotic/inflammatory panel, reveled up-regulated genes enriched for gluconeogenesis, fatty acid metabolism, M1 and M2 macrophages activation among others in CON-RET versus CON-SED (Figure 6C). Comparing RMS-RET to RMS-SED, three genes were up-regulated (*Dapk1, Tm6fs2 and Ptger4*) and three down-regulated (*Ccl2, Cd163 and Myd88*) (Figure 6D). The Top 10 GSA showed genes up-regulated for cytokine signaling, mammalian target of rapamycin (mTOR) and ECM degradation (Figure

6D). A total of 117 genes were up-regulated in RMS-SED vs CON-SED (Figure 6E, $p<0.05$). GSA revealed genes enriched for M1 and M2 activation, chemokine and interferon signaling, angiogenesis, and PDGF signaling, among other terms (Figure 6F). Biological process Gene Ontology (GO) term, based on the up-regulated genes showed genes involved mostly in immune cell activity in the RMS-SED compared to the CON-SED group (Figure 6G, FDR, adjusted p-value <0.05). Conversely, 124 genes were up-regulated and 1 down-regulated (*Ppara*) in RMS-RET vs CON-RET (Figure 6H, $p<0.05$). These genes were enriched for complement activation, collagen biosynthesis and modification, ECM degradation, and cytokine and chemokine signaling among other terms in the RMS-RET group (Figure 6I). Biological process GO term showed genes involved in immune system and collagen organization among others (Figure 6J, FDR, adjusted p-value <0.05).

Discussion

The overall objective of this study was to determine the extent to which RET can prevent the negative long-term consequences that RMS plus therapy exerts on skeletal muscle function and morphology specifically in a pediatric, preclinical model. Our main findings were that RET improved body composition and enhanced endurance performance, induced Type II myofibre hypertrophy, increased the number of several mononuclear cells involved in supporting muscle hypertrophy, and partially reversed the inflammatory/fibrotic gene signature induced by RMS plus therapy. These results suggest that RET-based interventions reduce the negative long-term, late effects of RMS plus therapy, in part by improving the skeletal muscle microenvironment. Excess adiposity and impaired physical performance leading to reduced participation in physical activity is commonly reported amongst cancer survivors (Irwin et al., 2003). We showed that RET is an effective form of voluntary training that leads to improved body composition and exercise performance. Adiposity did not increase in RET mice following RMS plus therapy while SED mice experienced an almost 2-fold increase in total body fat percentage which aligns with previous work from our group (D'Souza et al., 2019). Conversely, RET did not alter the increases in body weight and lean mass observed over the course of the study, likely due to the period of juvenile growth and development and the effects of RET on muscle hypertrophy not being detected by less sensitive whole-body measures. Adherence to exercise programs in cancer survivors is often a barrier to their efficacy (Courneya et al., 2005). Mice in the RET group effectively sustained the voluntary exercise protocol for eight weeks with increasing resistance. Daily distance travelled in our RMS plus therapy model was extremely similar to previous work in aged mice

(Dungan et al., 2019; Englund et al., 2020). Perhaps because of the excellent adherence to the RET protocol, mice in this group experienced a 200% increase in endurance performance despite RMS plus therapy. These results agree with previous literature from our group that describe increases in muscular performance in mouse models of cancer survivorship (Farber et al., 2021). In conclusion, these findings indicate that sustained adherence of RET leads to improvements in whole body composition and enhanced endurance performance in a model of RMS plus therapy.

Previous work has shown that RET causes myofibre hypertrophy and can lead to fibre type adaptations that favour a more oxidative profile in healthy and aged mice (Dungan et al., 2019; Englund et al., 2021). We confirm and extend these findings by showing that RET induces hypertrophy in both Type IIA and Type IIB myofibres, with a trend for an increase in Type IIX fibres and supports a shift from Type IIB to Type IIA fibres in a model of juvenile cancer survivorship. Taken together these data support the concept that a hybrid resistance-endurance exercise program can have beneficial dual effects of favouring enhanced endurance as well as leading to substantial muscular hypertrophy. Since many RMS survivors experience atrophy induced by both the disease and therapies, these preclinical findings support further investigation of these types of interventions in clinical studies.

Juvenile muscle growth requires functioning MuSCs with the addition of new nuclei to myofibres (Bachman et al., 2018). Previous work using the same RMS plus therapy model has shown that treatment-induced depletion of MuSCs underlies impaired muscle development (Paris et al., 2020). Further, RET has been shown to elevate MuSCs density followed eight weeks of training (Dungan et al., 2019), while MuSCs ablation impairs muscle adaptation to RET (Englund et al., 2021). Our results closely mirror these previous

findings showing that RMS plus therapy decreased MuSC number, while RET showed a trend to increase MuSC content in a model of juvenile cancer survivorship. Intriguingly, no changes in nuclei per fibre were found between groups; however, a significant increase in myonuclear domain was apparent in Type IIA fibres for RET mice compared to SED mice, as well as for Type IIX fibres in the control limb of RET compared to SED mice. This contrasts with previous work that reports increased number of myonuclei per fibre in RET versus SED groups in both young and aged mice (Dungan et al., 2019; Englund et al., 2021). This leads us to believe that the muscle hypertrophy seen in RET mice is driven primarily by protein synthesis, independent of myonuclear accretion. Indeed, our transcriptional profiling indicated an enrichment for genes involved in mTOR signaling responsible for activating muscle protein synthesis (Yoon, 2017). Further, these data suggest that the MuSC pool is still defective in RMS plus therapy even after an exercise intervention. It is possible that that these increases in domain size precede myonuclear addition from MuSCs and that a longer intervention may have resulted in an increase in myonuclei.

MuSCs are regulated by their local microenvironment which includes several cell types, including FAPs. FAPs regulate MuSC activation and differentiation and are the cellular source of fibro-fatty tissue accumulation in pathological conditions (Collao et al., 2020; Theret et al., 2021). Importantly, FAP depletion results in long long-term muscle atrophy (Wosczyna et al., 2019), and FAPs are a key source of paracrine factors that induce MuSC expansion necessary for muscle hypertrophy in models of increased muscle mechanical loading (Kaneshige et al., 2022). In line with previous work (Kallenbach et al., 2022), RMS plus therapy did not result in FAP depletion; however, we did observe a trend for a decrease in FAP number in RMS+Tx-SED versus CON-SED suggesting that

RMS+Tx may reduce FAP content. Interestingly, our transcriptional analysis revealed an enrichment in genes involved in platelet-derived growth factor (PDGF) signaling in RMS+Tx-SED compared to CON-SED. PDGF signaling is involved in sarcoma formation (Heldin, 2013); also known to promote fibrosis by inducing differentiation of mesenchymal cells into myofibroblasts, leading to excess ECM accumulation (Kendall & Feghali-Bostwick, 2014). Thus, the trend for FAP reduction by RMS plus therapy could be due to their myofibroblast differentiation, which is also observed in cardiac mesenchymal cells post-myocardial infraction (Hamid et al., 2022), that ultimately leads to the observed ECM accumulation in RMS+Tx. Interestingly, PDGF and Hedgehog signaling was down-regulated in the RMS+Tx-RET compared to RMS+Tx-SED. PDGF signaling in human FAPs have shown to promote proliferation and increase collagen production (Farup et al., 2021), while the Hedgehog pathway has been shown to induce profibrotic signaling that promotes myofibroblast differentiation and fibrosis in vivo (Horn et al., 2012), suggesting RET as a potential exercise intervention to decrease the fibrogenic fate of FAPs.

Conversely, we observed a significant increase in FAP content and proportion following RET in both CON and RMS plus therapy groups, which aligns with previous preclinical models of endurance exercise (D'Souza et al., 2019; Roubos et al., 2021; Saito et al., 2020), and resistance training studies in humans (Farup et al., 2015). Further, we detected more fibrosis in the RMS plus therapy condition with no effect of RET similar to our previous work with endurance exercise following radiation exposure (D'Souza et al., 2019). Hypertrophic stimuli induce ECM remodeling, by stimulating pathways involved in ECM degradation and synthesis which facilitates ECM reorganization, and promotes myofibre growth (Q. Zhang et al., 2014). Our transcriptomic data indicate ECM reorganization is ongoing in RET facilitated by diverse matrix metalloproteinases (*Mmp14,*

Mmp3, Mmp2, among others) and with collagen biosynthesis and modification and collagen degradation pathways both enriched in RMS+Tx-RET versus RMS+TxSED. Consistent with our results, Peck and colleagues showed that mechanical overload in mice increases the *Mmp14* gene signature, and that *Mmp14* gene expression was associated with an increase in skeletal muscle adaptation in humans following 14-weeks of progressive resistance exercise training (Peck et al., 2022).

Similarly, endothelial cells are a major component of the MuSC niche (Nederveen et al., 2017) and the perivascular location of FAPs suggest a strong communication with endothelial cells (Santini et al., 2020). Endothelial cell loss has been shown to be radiation dose-dependent, progressive over time (Archambeau et al., 1984), and contributes to myofibroblast activation and muscle fibrosis (Valle-Tenney et al., 2020). Evidence of dysfunctional FAP-endothelial cell crosstalk leading to fibrosis is evident from studies that genetically ablate FAPs following hind limb ischemia which results in impaired skeletal muscle revascularization and regeneration, leading to muscle fibrosis (Santini et al., 2020). In our RMS plus therapy model, a trend for fewer endothelial cells was detected which mirrors what was seen in FAPs. Similar to our FAP results, RET increased endothelial cell content and proportion, suggesting the pro-angiogenic effect of RET which could improve skeletal muscle capillarization and augment the cross-talk between endothelial cells and FAPs to promote muscle growth.

Previous work has suggested that long-term upregulation of inflammatory genes is involved in muscle degradation using the same RMS plus therapy model (Kallenbach et al., 2022). Similarly, we found an increase in cell abundance scores of macrophages and hematopoietic cells; supported by flow cytometry analysis that showed higher quantity of hematopoietic cells following RMS plus therapy, which aligned with an increase in the

inflammatory gene signature in skeletal muscle. Immune cells, especially macrophages have been involved not only as a key component of muscle regeneration but also in chronic inflammatory conditions (Tidball, 2017). Our study showed that RMS plus therapy increases genes related to M1 (pro-inflammatory) and M2 (anti-inflammatory) macrophage activation (i.e., *Ccr2*, *Ccl2*, and *Cxcr4*, among others) as well as genes involved in interferon signaling (i.e., *H2-Aa*, *Isg15a*, among others) and this heightened and prolonged inflammatory response aligns with previous work (Kallenbach et al., 2022). Excitingly, RET downregulated *Ccl2*, *Myd88,* and *Cd163* in RMS+Tx which are all genes involved in pro-inflammatory signaling. While RET in the CON limb showed higher M1 and M2 related genes than SED, this aligns with previous findings that show the necessity of macrophage recruitment to induce muscle hypertrophy following mechanical overload (DiPasquale et al., 2007). Thus, RET may inhibit the negative long-term late effects of RMS plus therapy by reducing inflammation.

Together, our results show that RET improves endurance performance, body composition, and induces skeletal muscle hypertrophy in a model of juvenile RMS plus therapy. These effects were mediated by positive changes in cellular dynamics, including increases in endothelial cells and FAPs and a partial reversal of the inflammatory and fibrotic gene signature. As such, our study indicates that skeletal muscles can adapt to RET following RMS plus therapy and suggests that increased protein synthesis and improvements in the muscle microenvironment may be the primary mechanisms responsible.

Figure Legends

Figure 1. Resistance endurance training improves endurance performance and body composition following RMS plus therapy.

(A) Study design. Four-week-old Male (n=10) and Female (n=10) C57Bl/6 mice received M3-9-M Rhabdomyosarcoma (RMS) cell injections into the left GAS to generate tumors with the right limb serving as an internal control (CON). After three days, all mice received systemic vincristine treatment administered by I.P. injection. Two days post-chemotherapy, mice were administered five doses of 4.8 Gy of gamma radiation localized to the left hindlimb only (RMS+Tx). Following treatment, mice were randomly divided into either sedentary (SED) or resistance endurance trained (RET) groups for eight weeks. Figure created via Biorender.com. (B) Average running distance (km/week) for RET mice throughout the intervention. (C) Endurance performance assessed by total distance run (m) until volitional exhaustion. (D) Average grip strength (grams/force). (E) Body weight (g). (F) Body fat percentage. (G) Lean mass (g). ***P < 0.001; SED vs RET. α = significantly different than baseline, Pre-Tx, Start-RET; β = significantly different than Month 1-RET; σ = significantly different than Month 2-RET. Three-way ANOVA, Sidak posthoc test. N = 7-9 per group.

Figure 2. ***RMS plus therapy induce muscle atrophy and fibrosis while RET restores relative muscle weight.***

(A) Muscle weight relative to total body weight (g). (B) Quantification of Trichrome stain for intramuscular fibrosis and collagen content as a % of total muscle area. Two-way ANOVA, Sidak post hoc tests. #P< 0.05 RMS and treated limb vs contralateral limb. N =

7-9 per group. (C) Representative images of Trichrome staining for intramuscular fibrosis and collagen content. Scale = 100 μm. *P < 0.05 SED vs RET. #P< 0.05 RMS+Tx vs. CON. Two-way ANOVA, Sidak posthoc test. N = 7-9 per group.

Figure 3. ***RMS plus therapy reduced Type IIB CSA and proportion while RET increased myofibre CSA and induced alterations in fibre type distribution independent of RMS plus therapy.***

(A) Representative image of myosin heavy chain stain immunofluorescence (Type IIA: green, Type IIB: orange, Type IIX: black, laminin: red). (B) Total fibre CSA (μm^2) (C) Average percentage of myofibres within each CSA (μm^2) bin in the CON limb. (D) Average percentage of myofibres within each CSA (μm^2) bin in the RMS+Tx limb. (E) Type IIA fibre specific CSA (μm^2). (F) Type IIB fibre specific CSA (μm^2). (G) Type IIX fibre specific CSA (μm^2). (H) Proportion of Type IIA fibres (% of total fibre #). (I) Proportion of Type IIB fibres (% of total fibre #). (J) Proportion of Type IIX fibres (% of total fibre #). *P < 0.05; SED vs RET group. ##P < 0.01; RMS+Tx vs CON. Two-way ANOVA, Sidak post hoc test or unpaired t-test for each bin (C and D). N=6-8 per group. Scale = 100 μm.

Figure 4. ***RET increases myonuclear domain with no changes in myonuclear accretion followed RMS plus therapy.***

(A) Representation of images used for quantifying myonuclei and myonuclear domain. (B) Myonuclear domain of all fibres (μm^2) (C) Type IIA fibre specific myonuclear domain (μm^2). (D) Type IIB fibre specific myonuclear domain (μm^2). (E) Type IIX fibre specific myonuclear domain (μm^2). (F) Total nuclei per fibre (#). (G) Nuclei per Type IIA fibre (#).

(H) Nuclei per Type IIB fibre (#) (I) Nuclei per Type IIX fibre (#). *P < 0.05, **P < 0.01, ***P < 0.001. Two-way ANOVA, Sidak post hoc test. N=6-8 per group. Scale = 100 μm.

Figure 5. ***RMS plus and resistance endurance training alter cellular dynamics in skeletal muscle.***

(A) Representative flow plots and gating strategy of cell populations analyzed from GAS. (B) Live cells per mg of muscle weight. (C) $CD45^+$ cells per mg of muscle and (D) percentage of $CD45^+$ cells gated. (E) $CD31^+$ cells per mg of muscle and (F) percentage of $CD31^+$ cells gated. (G) $\alpha7^+$ cells per mg of muscle and (H) percentage of $\alpha7^+$ cells gated (I) $Sca1^+$ cells per mg of muscle and (J) percentage of $Sca1^+$ cells gated. *P < 0.05, **P < 0.01; SED vs RET. #P < 0.05, ###P < 0.001; RMS+Tx vs CON. Two-way ANOVA, Sidak post hoc test. N = 7-9 per group.

Figure 6. ***Fibrotic and inflammatory signature is induced by RMS plus therapy and is partially reduced by resistance endurance training in skeletal muscle.***

(A) Multidimensional scaling (MDS) plot of CON-SED, CON-RET, RMS-SED, and RMS-RET transcription profile. (B) Cell profiler analysis identifying enrichment of mast cells, macrophages, and CD45 cells. (C) Volcano plot of $\log_2$-transformed fold change and $-\log_{10}$-transformed P values showing upregulated (in green) and downregulated (in purple) genes in CON-RET vs. CON-SED and the Top 10 direct enrichment score from the gene set analysis (GSA). (D) Volcano plot of $\log_2$transformed fold change and $-\log_{10}$-transformed P values showing upregulated (in green) and downregulated (in purple) genes in RMS-RET vs. RMS-SED and the Top 10 direct enrichment score from the gene set analysis (GSA). (E) Heatmap of differentially expressed genes (DEGs) in RMSSED vs. CON-SED. (F) Top 10 (GSA) in RMS-SED vs. CON-SED. (G) Top 10 Biological

process Gene Ontology (GO) terms (FDR, adjusted p-value) in RMS-SED vs. CON-SED. (H) Heatmap of DEGs in RMS-RET vs. CON-RET. (I) Top 10 GSA in RMS-RET vs. CON-RET. (J) Top 10 Biological process GO terms (FDR, adjusted p-value) in RMS-RET vs. CON-RET. N=3 per condition.

Figure 1.

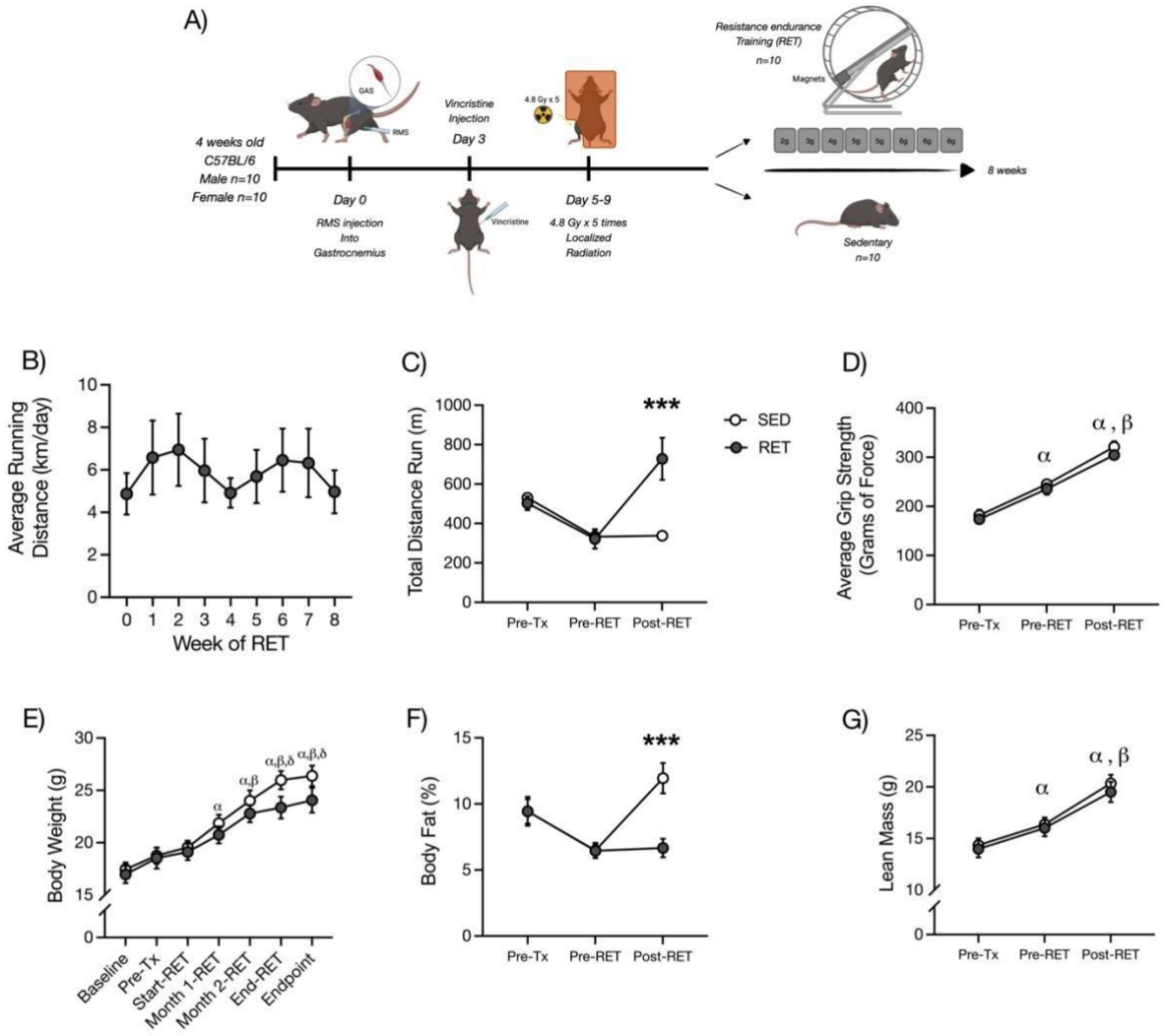
A)
Resistance endurance Training (RET) n=10
Magnets
GAS
RMS
4 weeks old C57BL/6 Male n=10 Female n=10
Vincristine Injection Day 3
4.8 Gy x 5
Day 0
RMS injection Into Gastrocnemius
Vincristine
Day 5-9
4.8 Gy x 5 times Localized Radiation
8 weeks
Sedentary n=10
B)
Average Running Distance (km/day)
Week of RET
C)
Total Distance Run (m)
***
SED
RET
Pre-Tx
Pre-RET
Post-RET
D)
Average Grip Strength (Grams of Force)
α
α , β
E)
Body Weight (g)
α
α,β
α,β,δ
Baseline
Pre-Tx
Start-RET
Month 1-RET
Month 2-RET
End-RET
Endpoint
F)
Body Fat (%)
G)
Lean Mass (g)

Figure 2.

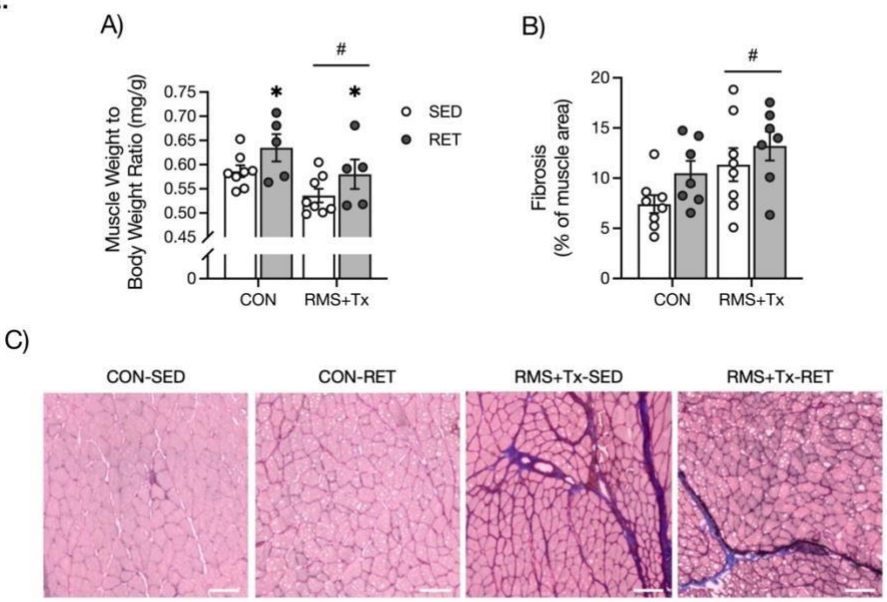
A)
Muscle Weight to Body Weight Ratio (mg/g)
0.75
0.70
0.65
0.60
0.55
0.50
0.45
0
*
*
#
SED
RET
CON
RMS+Tx
B)
Fibrosis (% of muscle area)
20
15
10
5
0
#
CON
RMS+Tx
C)
CON-SED
CON-RET
RMS+Tx-SED
RMS+Tx-RET

Figure 3.

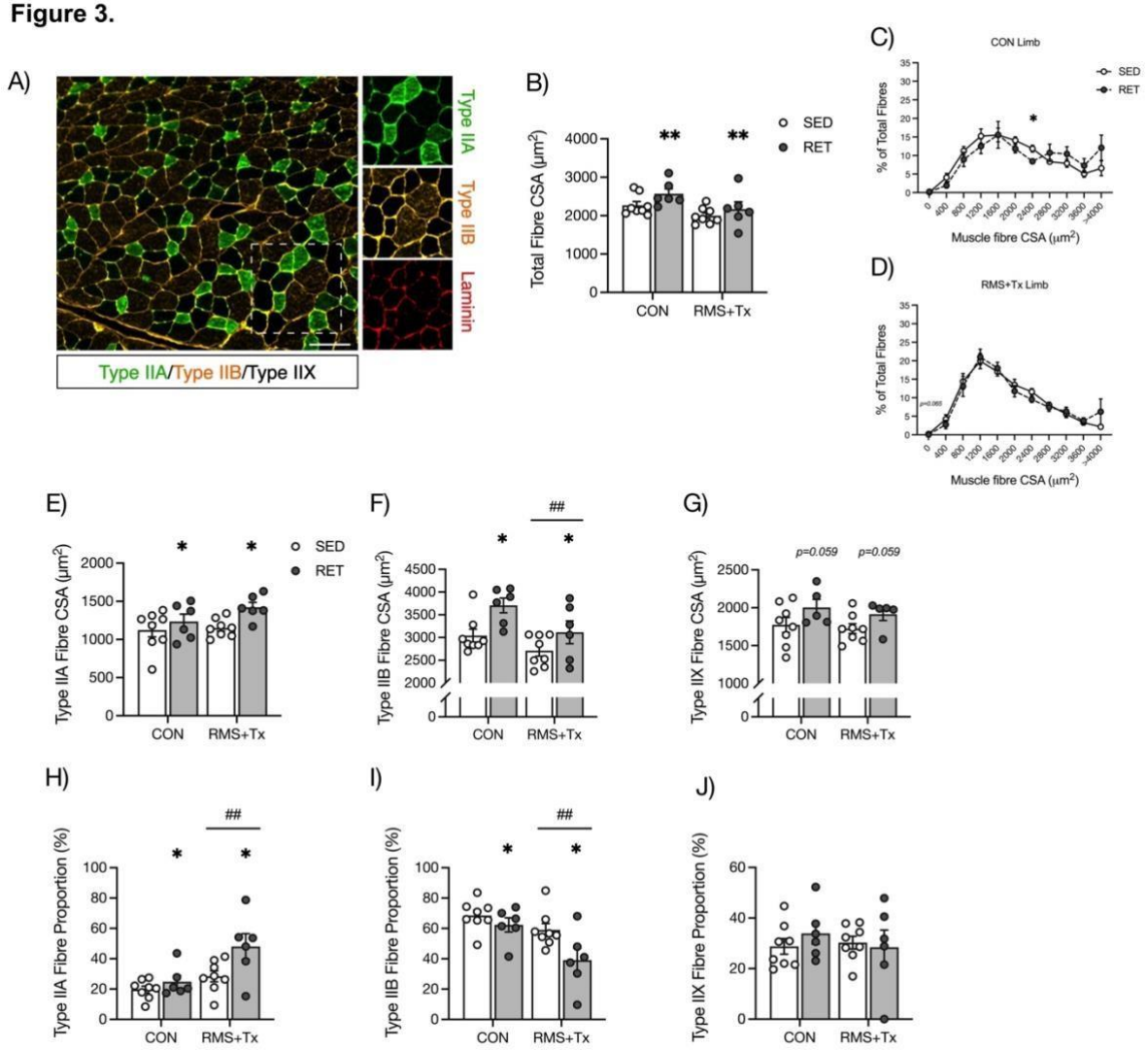
A)
Type IIA
Type IIB
Laminin
Type IIA/Type IIB/Type IIX
B)
Total Fibre CSA (μm²)
SED
RET
CON
RMS+Tx
C)
CON Limb
% of Total Fibres
Muscle fibre CSA (μm²)
D)
RMS+Tx Limb
E)
Type IIA Fibre CSA (μm²)
F)
Type IIB Fibre CSA (μm²)
G)
Type IIX Fibre CSA (μm²)
p=0.059
H)
Type IIA Fibre Proportion (%)
I)
Type IIB Fibre Proportion (%)
J)
Type IIX Fibre Proportion (%)

Figure 4.

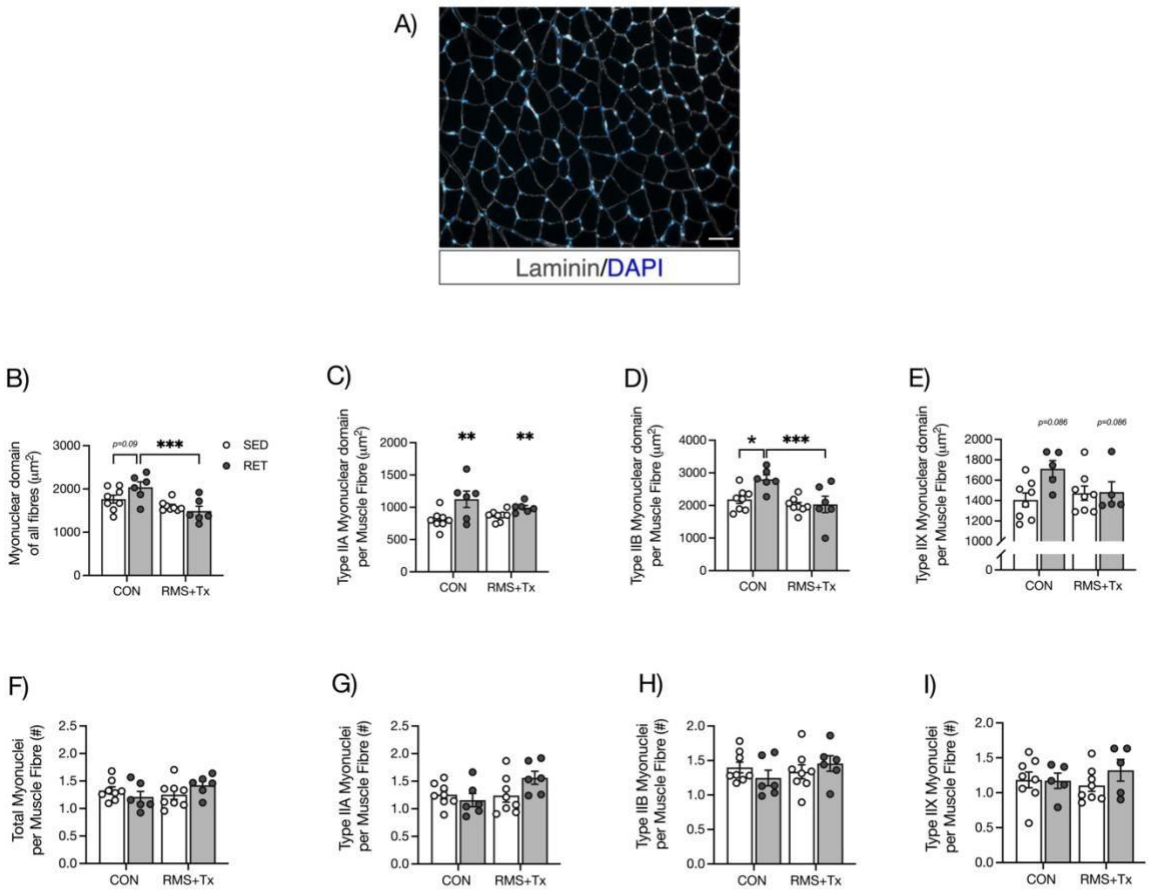
A)
Laminin/DAPI
B)
Myonuclear domain of all fibres (μm²)
SED
RET
p=0.09
***
CON
RMS+Tx
C)
Type IIA Myonuclear domain per Muscle Fibre (μm²)
**
**
D)
Type IIB Myonuclear domain per Muscle Fibre (μm²)
*
***
E)
Type IIX Myonuclear domain per Muscle Fibre (μm²)
p=0.086
p=0.086
F)
Total Myonuclei per Muscle Fibre (#)
G)
Type IIA Myonuclei per Muscle Fibre (#)
H)
Type IIB Myonuclei per Muscle Fibre (#)
I)
Type IIX Myonuclei per Muscle Fibre (#)

Figure 5.

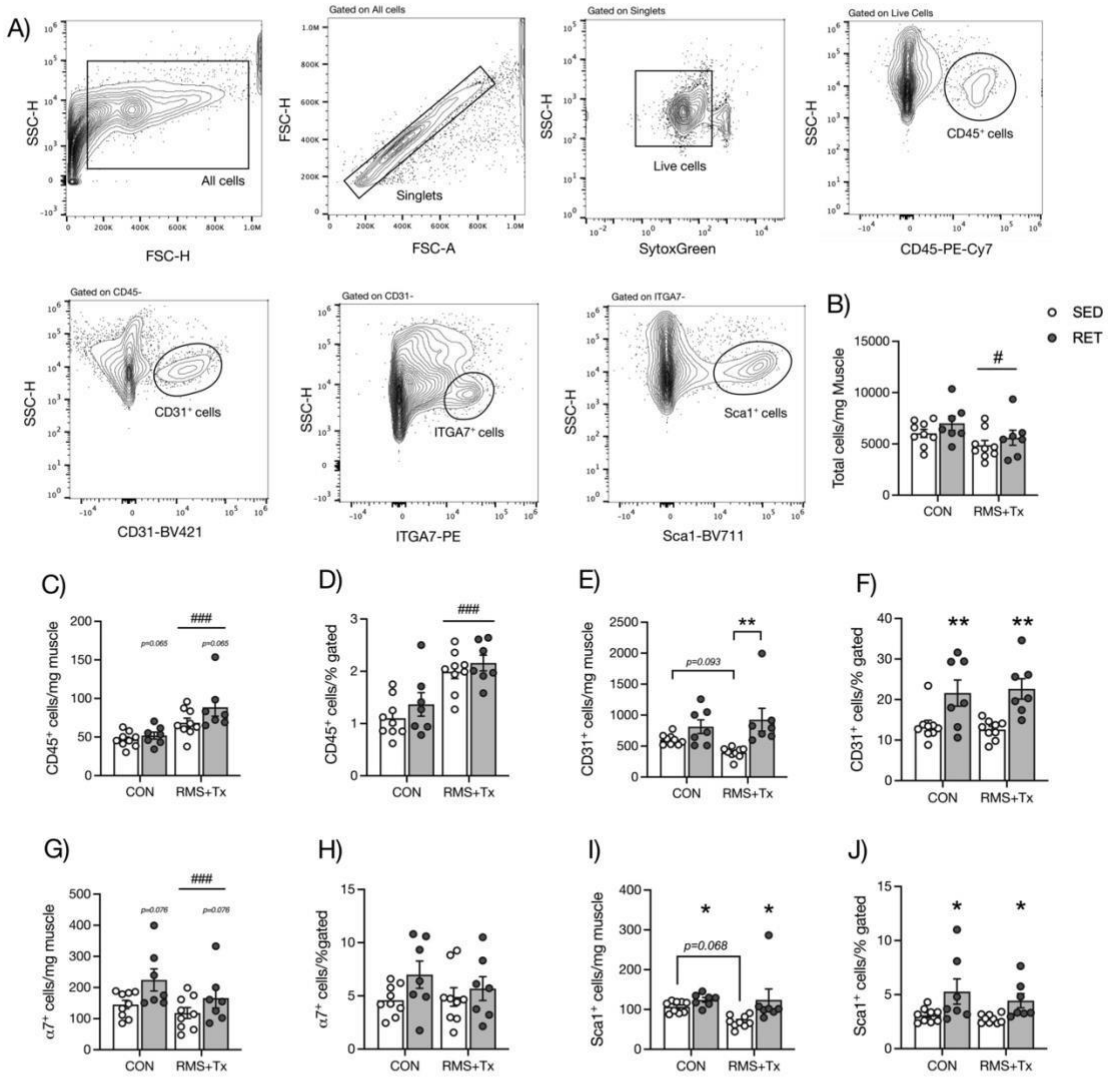
A)
Gated on All cells
Gated on Singlets
Gated on Live Cells
SSC-H
FSC-H
All cells
FSC-A
Singlets
SytoxGreen
Live cells
CD45-PE-Cy7
CD45⁺ cells
Gated on CD45-
Gated on CD31-
Gated on ITGA7-
CD31⁺ cells
CD31-BV421
ITGA7⁺ cells
ITGA7-PE
Sca1⁺ cells
Sca1-BV711
B)
SED
RET
Total cells/mg Muscle
CON
RMS+Tx
C)
CD45⁺ cells/mg muscle
D)
CD45⁺ cells/% gated
E)
CD31⁺ cells/mg muscle
F)
CD31⁺ cells/% gated
G)
α7⁺ cells/mg muscle
H)
α7⁺ cells/%gated
I)
Sca1⁺ cells/mg muscle
J)
Sca1⁺ cells/% gated

Figure 6.

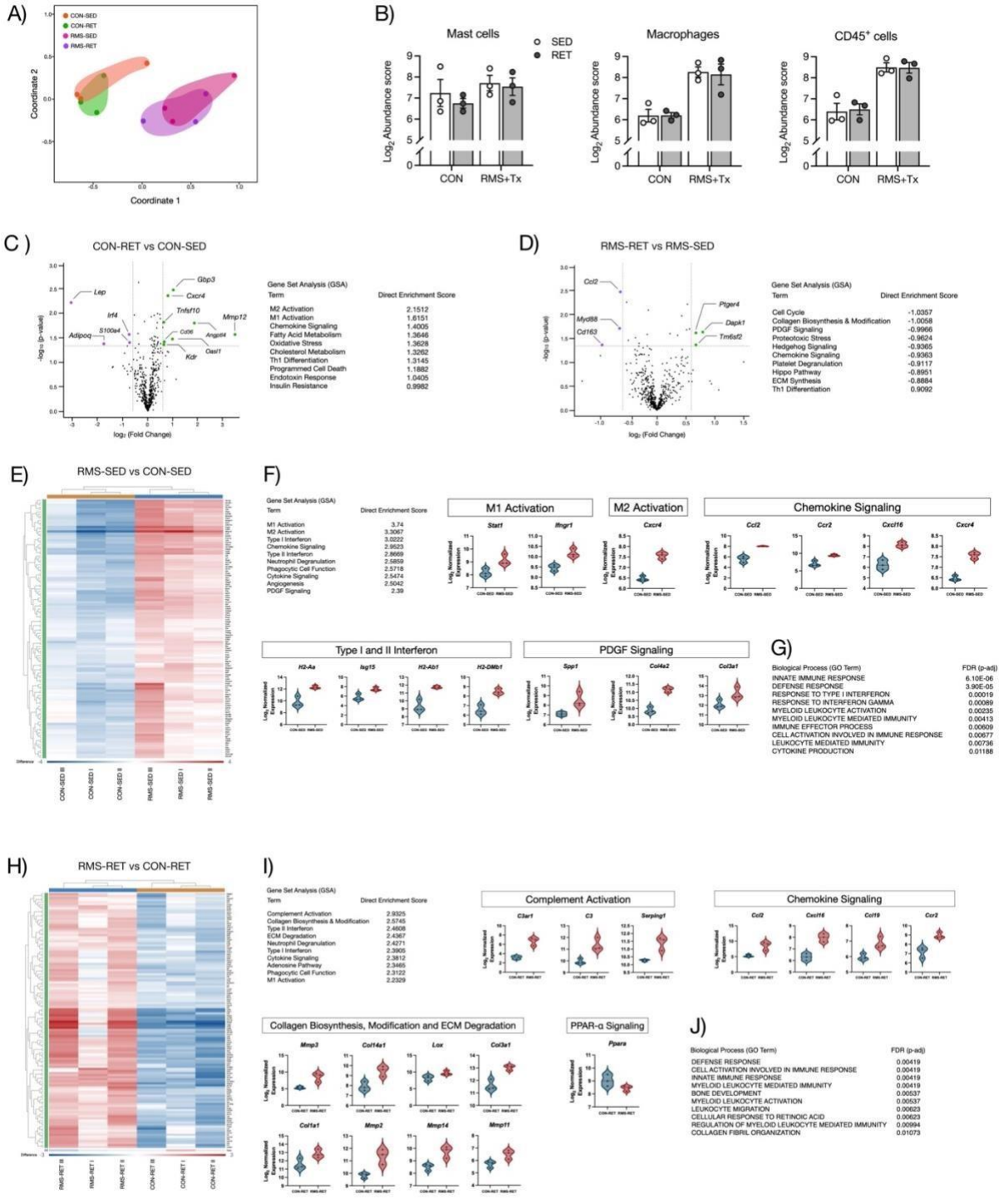
A)
CON-SED
CON-RET
RMS-SED
RMS-RET
Coordinate 1
Coordinate 2
B)
Mast cells
Macrophages
CD45+ cells
SED
RET
Log2 Abundance score
CON
RMS+Tx
C)
CON-RET vs CON-SED
Gene Set Analysis (GSA)
Term
Direct Enrichment Score
M2 Activation 2.1512
M1 Activation 1.6151
Chemokine Signaling 1.4005
Fatty Acid Metabolism 1.3646
Oxidative Stress 1.3628
Cholesterol Metabolism 1.3262
Th1 Differentiation 1.3145
Programmed Cell Death 1.1882
Endotoxin Response 1.0405
Insulin Resistance 0.9982
D)
RMS-RET vs RMS-SED
Gene Set Analysis (GSA)
Term
Direct Enrichment Score
Cell Cycle -1.0357
Collagen Biosynthesis & Modification -1.0058
PDGF Signaling -0.9966
Proteotoxic Stress -0.9624
Hedgehog Signaling -0.9365
Chemokine Signaling -0.9363
Platelet Degranulation -0.9117
Hippo Pathway -0.8951
ECM Synthesis -0.8884
Th1 Differentiation 0.9092
E)
RMS-SED vs CON-SED
F)
Gene Set Analysis (GSA)
Term
Direct Enrichment Score
M1 Activation 3.74
M2 Activation 3.3067
Type I Interferon 3.0222
Chemokine Signaling 2.9523
Type II Interferon 2.8669
Neutrophil Degranulation 2.5859
Phagocytic Cell Function 2.5718
Cytokine Signaling 2.5474
Angiogenesis 2.5042
PDGF Signaling 2.39
M1 Activation
M2 Activation
Chemokine Signaling
Type I and II Interferon
PDGF Signaling
G)
Biological Process (GO Term)
FDR (p-adj)
INNATE IMMUNE RESPONSE 6.10E-06
DEFENSE RESPONSE 3.90E-05
RESPONSE TO TYPE I INTERFERON 0.00019
RESPONSE TO INTERFERON GAMMA 0.00089
MYELOID LEUKOCYTE ACTIVATION 0.00235
MYELOID LEUKOCYTE MEDIATED IMMUNITY 0.00413
IMMUNE EFFECTOR PROCESS 0.00609
CELL ACTIVATION INVOLVED IN IMMUNE RESPONSE 0.00677
LEUKOCYTE MEDIATED IMMUNITY 0.00736
CYTOKINE PRODUCTION 0.01188
H)
RMS-RET vs CON-RET
I)
Gene Set Analysis (GSA)
Term
Direct Enrichment Score
Complement Activation 2.9325
Collagen Biosynthesis & Modification 2.5745
Type II Interferon 2.4608
ECM Degradation 2.4367
Neutrophil Degranulation 2.4271
Type I Interferon 2.3905
Cytokine Signaling 2.3812
Adenosine Pathway 2.3465
Phagocytic Cell Function 2.3122
M1 Activation 2.2329
Complement Activation
Chemokine Signaling
Collagen Biosynthesis, Modification and ECM Degradation
PPAR-α Signaling
J)
Biological Process (GO Term)
FDR (p-adj)
DEFENSE RESPONSE 0.00419
CELL ACTIVATION INVOLVED IN IMMUNE RESPONSE 0.00419
INNATE IMMUNE RESPONSE 0.00419
MYELOID LEUKOCYTE MEDIATED IMMUNITY 0.00419
BONE DEVELOPMENT 0.00537
MYELOID LEUKOCYTE ACTIVATION 0.00537
LEUKOCYTE MIGRATION 0.00623
CELLULAR RESPONSE TO RETINOIC ACID 0.00623
REGULATION OF MYELOID LEUKOCYTE MEDIATED IMMUNITY 0.00994
COLLAGEN FIBRIL ORGANIZATION 0.01073

Chapter III: Global Discussion

Rhabdomyosarcoma (RMS), an intramuscular soft-tissue cancer that is predominantly treated with a combination of chemoradiation therapy, is a disease that primarily affects children. Although this specific cancer is highly treatable, the primary concern that remains amongst survivors is how to ameliorate the multitude of long-term destructive effects that both the disease and its treatment have on skeletal muscle. Reduced functional performance of skeletal muscle as well as morphological fibre changes are both consequences of muscle atrophy and increased fibrotic deposition that accompanies the disease (Hartman et al., 2008; Paris et al., 2020; Stubblefield, 2011). This opens the door for novel therapeutic interventions to assist in reversing RMS associated muscle destruction. Opportunely, both resistance and endurance exercise have been proven to improve muscle integrity via SC activation and niche alterations that lead to direct increases in muscle CSA, performance, myonuclear characteristics, and increased vascularization (Christensen et al., 2014; Dungan et al., 2019; Kamel et al., 2020). Thus, the overall aim of this study was to determine whether RET was able to reverse the negative long-term muscle deficits of RMS on developing muscle by pairing novel models of RMS+therapy and murine progressive resistance endurance exercise. Specifically, we sought to uncover whether a) RET would lead to changes in muscle integrity/ performance as well as modifications to overall body composition b) what affect RET had on reversing muscle atrophy, specifically in relation to fibre-type adaptations in CSA as well as relative fibre-type proportions c) whether RET could induce changes in SC/progenitor number as well niche alterations that may affect inflammatory/fibrotic pathways.

We found that RET improved endurance performance with a concurrent reduction in total body fat percentage. Moreover, RET rescued muscle atrophy produced by RMS+therapy via an increase in GAS weight, while also stimulating Type II muscle fibre hypertrophy. A clear adaptation for Type IIA vs Type IIB fibres was evident in RET muscle, indicating a shift towards a more oxidative fibre profile. The deleterious effects of RMS were confirmed via increased intramuscular fibrosis, cell death, and immune cells number in the RMS+Tx limb. Together these data indicate that RET is a sustainable and effective way of increasing muscle health and performance in a preclinical pediatric murine model of Rhabdomyosarcoma.

It is well established by other groups that elevated myonuclear density is one primary mechanism behind increased hypertrophy with RET (Dungan et al., 2019; Englund et al., 2020). However, our results displayed an increase in myonuclear domain without increases in myonuclear number. It has been hypothesized by other groups that a specific level of muscle hypertrophy and domain expansion is required prior to stimulation of myonuclear accretion (Hikida et al., 1998; Kadi et al., 2004). Indeed, many studies have purported that increases in myonuclear number arise when skeletal muscle hypertrophy is enhanced by 26% (Hikida et al., 1998; Kadi et al., 2004; Kadi & Thornell, 2000; Roy et al., 1999). In fact, Kadi and colleagues (2004) have suggested that hypertrophy occurs without increases in myonuclear number until this specific threshold of hypertrophy is surpassed. In our study, all of the hypertrophy witnessed in the RET group was below this 26% threshold with reported increases in Type IIA fibres of 8.6% in the CON limb and 21% in the treated limb, increases in Type IIX fibres of 14% in the CON

limb and 19% in the treated limb, and increases in Type IIB fibres of 20% in the CON limb and 19% in the treated limb. Collectively, these results suggest that the hypertrophic threshold at which gains in myonuclear number occur had not been achieved, providing a possible explanation for the lack of myonuclear accretion and corroborating previous work. Conclusively, this lack of myonuclear accretion suggests that myonuclear donation is dependent on relative level of hypertrophy and increases in myonuclear domain size. This leaves an interesting avenue for other research to explore what weight of resistance/length of training period is required (using this voluntary wheel running protocol in a cancer treated juvenile population) to induce a shift towards myonuclear accretion and hypertrophy via SC fusion.

Likewise, it has been demonstrated by others that the GAS is predominantly comprised of Type II fibres (Edgerton et al., 1975; Gollnick et al., 1974). Moreover, a recent study demonstrated that fibre distribution was dependent on location within the muscle, citing an abundance of Type IIB fibres along the periphery of the muscle and a concentration of Type IIA and Type IIX located within the belly of the muscle (Sawano et al., 2016). Furthermore, they found a propensity for Type I fibre accumulation in the soleus, with a corresponding scarcity of Type I fibres found in the GAS muscle (Sawano et al., 2016). Similar to previous work, we observed that there was a relatively small portion of Type I fibres present in the mouse GAS. In the RET group, all RMS+Tx muscles possessed Type I fibres, yet only 2.8% of all fibres were Type I. However, only half of the CON-RET muscles contained Type I fibres, and only 1.6% of the analyzed fibres were Type I. Similarly, in the SED group, 87.5% of RMS+Tx muscles had Type I fibres present, and of this 1.6% of all fibres analyzed were Type I. Lastly, CON-SED limbs contained Type I fibres, however only 1.9% of these fibres were Type I. Due to the infrequency in

Type I fibre appearance, Type I fibre-specific assessments including CSA, myonuclear domain and myonuclear number were excluded from analyses and our focus was directed to Type II fibre measures. Future work looking to characterize morphological fibre changes across all fibre types would benefit from taking samples from a diverse range of muscles recruited that are known to contain a higher percentage of Type I fibres (i.e., Extensor digitorum longus, vastus lateralis, plantaris etc.) The main limitation of the present study is that we did not include a control group of mice which did not receive treatment. Instead, we chose a within subject control in the form of a contralateral control limb. This design was chosen because there is already extensive research that has looked at muscle atrophy and restructuring, SC dynamics, and whole-body performance after chemoradiation, as well as studies that have focused on the exact RET protocol we used on healthy young mice (Bachman et al., 2020; Dungan et al., 2019; Englund et al., 2021; Paris et al., 2020). When compared to this current study, other studies that used older healthy mice reported greater total distance run on the wheels, but almost identical increases in muscle CSA and fibre-type adaptations. Although this study using an older, healthy cohort reported an increase in myonuclear accretion, the lack of satellite cell donation seen in our work can in part be explained by the reduction in satellite cell number and function after radiation and chemotherapy as shown in previous work that focused exclusively on the effects of chemoradiation and RMS without exercise.

Another limitation of the study was that we focused solely on the GAS muscle. Since this is a primary force producing muscle of the lower limb during voluntary wheel running, we were justified in our choice. Further rationale for using the GAS was to guarantee specificity of the tumor injection and the treatment. The GAS is a large, superficial muscle which allowed us to target the RMS injection specifically to muscle and

localize the radiation dose to the left lower hind limb. However, a larger scope of total muscle health could have been possible if we had analyzed other muscles in the leg such as the EDL and plantaris muscles (Dungan et al., 2019; Englund et al., 2021; Paris et al., 2020). We originally excised the synergistic soleus to examine which has a greater proportion of Type I fibres. However due to the lack of tissue, we were unable to perform analyses on this muscle and therefore chose to only focus on the GAS.

Another limitation was the attrition rate of the mice in both RET and SED groups. One female and two male mice in the RET group and one male mouse in the SED group reached endpoint before cessation of the exercise protocol. These untimely deaths were due in part to tumor recurrence in the hindlimb injected with the M3-9-M cells. As such, we excluded wheel running and anthropometric data collected prior to death for these mice. If these mice had survived, it may have allowed for greater insight into potential differences between RET and SED groups and provided sufficient statistical power for sex-based comparisons. In fact, follow-up studies that focus on sex-based comparisons should be done to determine if the degree of hypertrophy, fibre-type shift, and body recomposition are similar in males and females. Minor sex-based differences in the muscle-protein synthesis response have been noted by different groups (Burd et al., 2009; West et al., 2012), yet others have suggested that SC responses to both acute and chronic resistance training occur irrespective of sex (Abou Sawan et al., 2021). Furthermore, measuring food intake and chow composition (i.e., variable diets of high protein, high fat, and control) with respect to body composition as well as using an infusion of amino acid tracer to measure muscle protein synthesis would be useful especially in a cancer model where loss of total body mass (cachexia) is prevalent, and food-intake is known to diminish. Earlier work from our group has confirmed that diet-induced obesity increased

muscle fibrosis and adiposity compared to controls post-radiation (D'Souza et al., 2019), and so manipulating food composition to induce obesity would provide the means to explore the effect of obesity on intramuscular fibrosis and fibre hypertrophy. Thus, monitoring food consumption trends, inflammatory markers in the niche, levels of muscle hypertrophy, intramuscular adiposity and muscle protein synthesis after being assigned to one of the 3 diet conditions could serve as the basis for further experimentation into diet-induced muscle/niche health, body composition and muscular function following RET in a RMS treated murine model.

Our current findings provide the basis for future work to investigate practical therapeutic interventions for hybrid exercise in a pediatric RMS survivor population. We show that in this design of localized tumor burden and treatment, RET can be sustained for the full 8-week duration and successfully stimulates muscle fibre growth. An interesting direction would be to see if similar adherence to an 8-week hybrid training protocol that combined elements of both resistance and endurance is sustainable in the juvenile clinical population, and if so what the appropriate frequency and intensity for this specific form of hybrid training would be to achieve maximum muscular benefits. The extremely pertinent and topical issue of mental health in juvenile cancer survivorship would be an interesting variable to consider in combination with RET. Indeed, many cancer survivors show decreased physical activity and adherence to exercise interventions (Rogers et al., 2006, 2008), and thus indicators of improved mental health, feelings of resiliency, and changes to overall outlook on physical activity could be compared between exercise and non-exercise juvenile cancer groups. This may prove an important variable to consider, especially if such changes in attitude towards exercise are able to modify physical activity

behaviour later in life, since we know that the damaging effects on muscle from early childhood cancer treatment persist well into adulthood.

Although this RMS+RET model sheds light into the longer-term benefits of exercise into early adulthood, detraining effects in a survivorship study could be used to understand if muscle adaptations and performance improvements continued to persist and if survival rates were affected after cessation of therapy/ RET. Other groups have shown a decrease in CSA in detrained healthy adult mice (<16% vs immediately post-training), and a corresponding decrease in myonuclear/SC density in detrained mice similar to untrained controls (Dungan et al., 2019). Yet no studies have assessed whether these detraining effects remain consistent in a juvenile cancer treated population. From a mechanistic perspective, there is still much to uncover regarding the pro-fibrotic role of FAPs in exacerbating intramuscular fibrosis in juvenile cancer patients. Our research showed a clear increase in intramuscular fibrosis in the RMS+Tx leg: however, further work should be done in order to understand the mechanism behind this fibrotic deposition, including FAP signaling and upstream pathways that may lead to fibro-adipogenic differentiation of FAPs. We know that FAPs aid SCs under homeostatic conditions to repair skeletal muscle following exercise via pro-differentiation signaling and that they are necessary for muscle maintenance in healthy populations (Boppart et al., 2013; Joe et al., 2010). However, the role of exercise on attenuating the pathogenic, fibro-adipogenic lineage commitment in the juvenile cancer population remains unknown. The findings from our study extend our knowledge on how chemoradiation treatment of RMS impacts muscle health, and the effects that RET has on mitigating these consequences. In conclusion, we demonstrate that voluntary RET can preserve muscle health and function after treatment of RMS.

Chapter IV: Statement of Contribution

OS, NC, and MD contributed to the study design and direction. OS and NC performed experiments. OS, NC, and TC contributed to analysis. OS, NC and MD wrote the manuscript with contributions from other authors.

Chapter V: References

Abou Sawan, S., Hodson, N., Babits, P., Malowany, J. M., Kumbhare, D., & Moore, D. R. (2021). Satellite cell and myonuclear accretion is related to training-induced skeletal muscle fiber hypertrophy in young males and females. *Journal of Applied Physiology*, *131*(3), 871–880. https://doi.org/10.1152/japplphysiol.00424.2021

Alexa A, Rahnenfuhrer J. topGO: Enrichment Analysis for Gene Ontology. R package version 1.38.1 (2019). (n.d.).

Al-Majid, S., & McCarthy, D. O. (2001). Cancer-Induced Fatigue and Skeletal Muscle Wasting: The Role of Exercise. *Biological Research For Nursing*, *2*(3), 186–197. https://doi.org/10.1177/109980040100200304

Alves, M. J., Figuerêdo, R. G., Azevedo, F. F., Cavallaro, D. A., Neto, N. I. P., Lima, J. D. C., MatosNeto, E., Radloff, K., Riccardi, D. M., Camargo, R. G., De Alcântara, P. S. M., Otoch, J. P., Junior, M. L. B., & Seelaender, M. (2017). Adipose tissue fibrosis in human cancer cachexia: The role of TGFβ pathway. *BMC Cancer*, *17*(1), 190. https://doi.org/10.1186/s12885-017-3178-8

Archambeau, J. O., Ines, A., & Fajardo, L. F. (1984). Response of swine skin microvasculature to acute single exposures of X rays: Quantification of endothelial changes. *Radiation Research*, *98*(1), 37–51.

Armstrong, G. T., Kawashima, T., Leisenring, W., Stratton, K., Stovall, M., Hudson, M. M., Sklar, C. A., Robison, L. L., & Oeffinger, K. C. (2014). Aging and Risk of Severe, Disabling, LifeThreatening, and Fatal Events in the Childhood Cancer

Survivor Study. *Journal of Clinical Oncology*, *32*(12), 1218–1227. https://doi.org/10.1200/JCO.2013.51.1055

Bachman, J. F., Blanc, R. S., Paris, N. D., Kallenbach, J. G., Johnston, C. J., Hernady, E., Williams, J. P., & Chakkalakal, J. V. (2020). Radiation-Induced Damage to Prepubertal Pax7+ Skeletal Muscle Stem Cells Drives Lifelong Deficits in Myofiber Size and Nuclear Number. *IScience*, *23*(11), 101760. https://doi.org/10.1016/j.isci.2020.101760

Bachman, J. F., & Chakkalakal, J. V. (2021). Insights into muscle stem cell dynamics during postnatal development. *The FEBS Journal*, *n/a*(n/a). https://doi.org/10.1111/febs.15856

Bachman, J. F., Klose, A., Liu, W., Paris, N. D., Blanc, R. S., Schmalz, M., Knapp, E., & Chakkalakal, J. V. (2018). Prepubertal skeletal muscle growth requires Pax7-expressing satellite cell-derived myonuclear contribution. *Development*, *145*(20). https://doi.org/10.1242/dev.167197

Birbrair, A., Zhang, T., Wang, Z.-M., Messi, M. L., Enikolopov, G. N., Mintz, A., & Delbono, O. (2013). Role of Pericytes in Skeletal Muscle Regeneration and Fat Accumulation. *Stem Cells and Development*, *22*(16), 2298–2314. https://doi.org/10.1089/scd.2012.0647

Boppart, M. D., De Lisio, M., Zou, K., & Huntsman, H. D. (2013). Defining a role for non-satellite stem cells in the regulation of muscle repair following exercise. *Frontiers in Physiology*, *4*. https://doi.org/10.3389/fphys.2013.00310

Bourdon, A., Grandy, S. A., & Keats, M. R. (2018). Aerobic exercise and cardiopulmonary fitness in childhood cancer survivors treated with a cardiotoxic agent: A meta-analysis. *Supportive Care in Cancer*, *26*(7), 2113–2123. https://doi.org/10.1007/s00520-018-4208-z

Braam, K. I., van der Torre, P., Takken, T., Veening, M. A., van Dulmen-den Broeder, E., & Kaspers, G. J. L. (2016). Physical exercise training interventions for children and young adults during and after treatment for childhood cancer. *The Cochrane Database of Systematic Reviews*, *3*, CD008796. https://doi.org/10.1002/14651858.CD008796.pub3

Burd, N. A., Tang, J. E., Moore, D. R., & Phillips, S. M. (2009). Exercise training and protein metabolism: Influences of contraction, protein intake, and sex-based differences. *Journal of Applied Physiology*, *106*(5), 1692–1701. https://doi.org/10.1152/japplphysiol.91351.2008

Campbell, K. L., Winters-Stone, K. M., Wiskemann, J., May, A. M., Schwartz, A. L., Courneya, K. S., Zucker, D. S., Matthews, C. E., Ligibel, J. A., Gerber, L. H., Morris, G. S., Patel, A. V., Hue, T. F., Perna, F. M., & Schmitz, K. H. (2019). Exercise Guidelines for Cancer Survivors: Consensus Statement from International Multidisciplinary Roundtable. *Medicine and Science in Sports and Exercise*, *51*(11), 2375–2390. https://doi.org/10.1249/MSS.0000000000002116

Canadian Cancer Society. (2021). *Rhabdomyosarcoma—Survival statistics*.

Cave, J., Paschalis, A., Huang, C. Y., West, M., Copson, E., Jack, S., & Grocott, M. P. W. (2018). A systematic review of the safety and efficacy of aerobic exercise

during cytotoxic chemotherapy treatment. *Supportive Care in Cancer*, *26*(10), 3337–3351. https://doi.org/10.1007/s00520-018-4295-x

Chen, C., Dorado Garcia, H., Scheer, M., & Henssen, A. G. (2019). Current and Future Treatment Strategies for Rhabdomyosarcoma. *Frontiers in Oncology*, *9*, 1458. https://doi.org/10.3389/fonc.2019.01458

Chen, Y., Jungsuwadee, P., Vore, M., Butterfield, D. A., & St. Clair, D. K. (2007). Collateral Damage in Cancer Chemotherapy: Oxidative Stress in Nontargeted Tissues. *Molecular Interventions*, *7*(3),147. https://doi.org/10.1124/mi.7.3.6

Christensen, J. F., Jones, L. W., Tolver, A., Jørgensen, L. W., Andersen, J. L., Adamsen, L., Højman, P., Nielsen, R. H., Rørth, M., & Daugaard, G. (2014). Safety and efficacy of resistance training in germ cell cancer patients undergoing chemotherapy: A randomized controlled trial. *British Journal of Cancer*, *111*(1), 8–16. https://doi.org/10.1038/bjc.2014.273

Cieśla, M., Dulak, J., & Józkowicz, A. (2014). MicroRNAs and epigenetic mechanisms of rhabdomyosarcoma development. *The International Journal of Biochemistry & Cell Biology*, *53*, 482–492. https://doi.org/10.1016/j.biocel.2014.05.003

Clifford, B., Koizumi, S., Wewege, M. A., Leake, H. B., Ha, L., Macdonald, E., Fairman, C. M., & Hagstrom, A. D. (2021). The Effect of Resistance Training on Body Composition During and After Cancer Treatment: A Systematic Review and Meta-Analysis. *Sports Medicine (Auckland, N.Z.)*, *51*(12), 2527–2546. https://doi.org/10.1007/s40279-021-01542-6

Collao, N., Farup, J., & De Lisio, M. (2020). Role of Metabolic Stress and Exercise in Regulating Fibro/Adipogenic Progenitors. *Frontiers in Cell and Developmental Biology*, *8*. https://doi.org/10.3389/fcell.2020.00009

Cosgrove, B. D., Gilbert, P. M., Porpiglia, E., Mourkioti, F., Lee, S. P., Corbel, S. Y., Llewellyn, M. E., Delp, S. L., & Blau, H. M. (2014). Rejuvenation of the aged muscle stem cell population restores strength to injured aged muscles. *Nature Medicine*, *20*(3), 255–264. https://doi.org/10.1038/nm.3464

Courneya, K. S., Friedenreich, C. M., Quinney, H. A., Fields, A. L. A., Jones, L. W., Vallance, J. K. H., & Fairey, A. S. (2005). A longitudinal study of exercise barriers in colorectal cancer survivors participating in a randomized controlled trial. *Annals of Behavioral Medicine: A Publication of the Society of Behavioral Medicine*,*29*(2), 147–153. https://doi.org/10.1207/s15324796abm2902_9

Courneya, K. S., Segal, R. J., Mackey, J. R., Gelmon, K., Reid, R. D., Friedenreich, C. M., Ladha, A. B., Proulx, C., Vallance, J. K. H., Lane, K., Yasui, Y., & McKenzie, D. C. (2007). Effects of Aerobic and Resistance Exercise in Breast Cancer Patients Receiving Adjuvant Chemotherapy: A Multicenter Randomized Controlled Trial. *Journal of Clinical Oncology*, *25*(28), 4396–4404. https://doi.org/10.1200/JCO.2006.08.2024

Cramer, A. A. W., Prasad, V., Eftestøl, E., Song, T., Hansson, K.-A., Dugdale, H. F., Sadayappan, S., Ochala, J., Gundersen, K., & Millay, D. P. (2020). Nuclear numbers in syncytial muscle fibers promote size but limit the development of larger myonuclear domains. *Nature Communications*, *11*. https://doi.org/10.1038/s41467-020-20058-7

Dagher, R., & Helman, L. (1999). Rhabdomyosarcoma: An Overview. *The Oncologist*, *4*(1), 34–44. https://doi.org/10.1634/theoncologist.4-1-34

De Lisio, M., Jensen, T., Sukiennik, R. A., Huntsman, H. D., & Boppart, M. D. (2014). Substrate and strain alter the muscle-derived mesenchymal stem cell secretome to promote myogenesis. *Stem Cell Research & Therapy*, *5*(3), 74. https://doi.org/10.1186/scrt463

De Lisio, M., Kaczor, J. J., Phan, N., Tarnopolsky, M. A., Boreham, D. R., & Parise, G. (2011). Exercise training enhances the skeletal muscle response to radiation-induced oxidative stress. *Muscle & Nerve*, *43*(1), 58–64. https://doi.org/10.1002/mus.21797

De Ruysscher, D., Niedermann, G., Burnet, N. G., Siva, S., Lee, A. W. M., & Hegi-Johnson, F. (2019). Radiotherapy toxicity. *Nature Reviews. Disease Primers*, *5*(1), 13. https://doi.org/10.1038/s41572-019-0064-5

Del Fabbro, E., Inui, A., & Strasser, F. (2012). Overview of cancer cachexia. In E. Del Fabbro, A. Inui, & F. Strasser (Eds.), *Cancer Cachexia* (pp. 1–5). Springer Healthcare Ltd. https://doi.org/10.1007/978-1-910315-07-1_1

Dewys, W. D., Begg, C., Lavin, P. T., Band, P. R., Bennett, J. M., Bertino, J. R., Cohen, M. H., Douglass, H. O., Engstrom, P. F., Ezdinli, E. Z., Horton, J., Johnson, G. J., Moertel, C. G., Oken, M. M., Perlia, C., Rosenbaum, C., Silverstein, M. N., Skeel, R. T., Sponzo, R. W., & Tormey, D. C. (1980). Prognostic effect of weight loss prior tochemotherapy in cancer patients. *The American Journal of Medicine*, *69*(4), 491–497. https://doi.org/10.1016/S0149-2918(05)80001-3

DiPasquale, D. M., Cheng, M., Billich, W., Huang, S. A., van Rooijen, N., Hornberger, T. A., & Koh, T. J. (2007). Urokinase-type plasminogen activator and macrophages are required for skeletal muscle hypertrophy in mice. *American Journal of Physiology. Cell Physiology*, *293*(4), C1278-1285. https://doi.org/10.1152/ajpcell.00201.2007

Dos Santos, W. D. N., Vieira, A., de Lira, C. A. B., Mota, J. F., Gentil, P., de Freitas Junior, R., Battaglini, C. L., Bottaro, M., & Vieira, C. A. (2019). Once a Week Resistance Training Improves Muscular Strength in Breast Cancer Survivors: A Randomized Controlled Trial. *Integrative Cancer Therapies*, *18*. https://doi.org/10.1177/1534735419879748

Dracham, C. B., Shankar, A., & Madan, R. (2018). Radiation induced secondary malignancies: A review article. *Radiation Oncology Journal*, *36*(2), 85–94. https://doi.org/10.3857/roj.2018.00290

D'Souza, D., Roubos, S., Larkin, J., Lloyd, J., Emmons, R., Chen, H., & De Lisio, M. (2019). The Late Effects of Radiation Therapy on Skeletal Muscle Morphology and Progenitor Cell Content are Influenced by Diet-Induced Obesity and Exercise Training in Male Mice. *Scientific Reports*, *9*(1), 6691.https://doi.org/10.1038/s41598-019-43204-8

Dungan, C. M., Murach, K. A., Frick, K. K., Jones, S. R., Crow, S. E., Englund, D. A., Vechetti, I. J., Figueiredo, V. C., Levitan, B. M., Satin, J., McCarthy, J. J., & Peterson, C. A. (2019). Elevated myonuclear density during skeletal muscle hypertrophy in response to training is reversed during detraining. *American*

Journal of Physiology-Cell Physiology, *316*(5), C649–C654. https://doi.org/10.1152/ajpcell.00050.2019

Dyar, K. A., Ciciliot, S., Wright, L. E., Biensø, R. S., Tagliazucchi, G. M., Patel, V. R., Forcato, M., Paz, M. I. P., Gudiksen, A., Solagna, F., Albiero, M., Moretti, I., Eckel-Mahan, K. L., Baldi, P., Sassone-Corsi, P., Rizzuto, R., Bicciato, S., Pilegaard, H., Blaauw, B., & Schiaffino, S. (2014). Muscle insulin sensitivity and glucose metabolism are controlled by the intrinsic muscle clock. *Molecular Metabolism*, *3*(1), 29–41. https://doi.org/10.1016/j.molmet.2013.10.005

Edgerton, V. R., Smith, J. L., & Simpson, D. R. (1975). Muscle fibre type populations of human leg muscles. *The Histochemical Journal*, *7*(3), 259–266.https://doi.org/10.1007/BF01003594

Emmons, R., Ngu, M., Xu, G., Hernández-Saavedra, D., Chen, H., & DE Lisio, M. (2019). Effects of Obesity and Exercise on Bone Marrow Progenitor Cells after Radiation. *Medicine and Science in Sports and Exercise*, *51*(6), 1126–1136. https://doi.org/10.1249/MSS.0000000000001894

Englund, D. A., Figueiredo, V. C., Dungan, C. M., Murach, K. A., Peck, B. D., Petrosino, J. M., Brightwell, C. R., Dupont, A. M., Neal, A. C., Fry, C. S., Accornero, F., McCarthy, J. J., & Peterson, C. A. (2021). Satellite Cell Depletion Disrupts Transcriptional Coordination and Muscle Adaptation to Exercise. *Function*, *2*(1). https://doi.org/10.1093/function/zqaa033

Englund, D. A., Murach, K. A., Dungan, C. M., Figueiredo, V. C., Vechetti, I. J., Dupont-Versteegden, E. E., McCarthy, J. J., & Peterson, C. A. (2020). Depletion of resident muscle stem cells negatively impacts running volume, physical function,

and muscle fiber hypertrophy in response to lifelong physical activity. *American Journal of Physiology. Cell Physiology*, *318*(6), C1178–C1188. https://doi.org/10.1152/ajpcell.00090.2020

Farber, E., Kwiecien, J. M., Bojic, D., Ngu, M., Akohene-Mensah, P., Vanhie, J. J., Lloyd, J., Larkin, J., & De Lisio, M. (2021). Exercise Improves Cancer-free Survival and Health Span in a Model of Radiation-induced Cancer. *Medicine & Science in Sports & Exercise*, *53*(11), 2254–2263. https://doi.org/10.1249/MSS.0000000000002711

Farup, J., De Lisio, M., Rahbek, S. K., Bjerre, J., Vendelbo, M. H., Boppart, M. D., & Vissing, K. (2015). Pericyte response to contraction mode-specific resistance exercise training in human skeletal muscle. *Journal of Applied Physiology (Bethesda, Md.: 1985)*, *119*(10), 1053–1063. https://doi.org/10.1152/japplphysiol.01108.2014

Farup, J., Just, J., de Paoli, F., Lin, L., Jensen, J. B., Billeskov, T., Roman, I. S., Cömert, C., Møller, A. B., Madaro, L., Groppa, E., Fred, R. G., Kampmann, U., Gormsen, L. C., Pedersen, S. B., Bross, P., Stevnsner, T., Eldrup, N., Pers, T. H., … Jessen, N. (2021). Human skeletal muscle CD90+ fibro-adipogenic progenitors are associated with muscle degeneration in type 2 diabetic patients. *Cell Metabolism*, *33*(11), 2201-2214.e11. https://doi.org/10.1016/j.cmet.2021.10.001

Feige, P., & Rudnicki, M. A. (2020). Isolation of satellite cells and transplantation into mice for lineage tracing in muscle. *Nature Protocols*, *15*(3), 1082–1097. https://doi.org/10.1038/s41596-019-0278-8

Fiddler, T. A., Smith, L., Tapscott, S. J., & Thayer, M. J. (1996). Amplification of MDM2 inhibits MyoD-mediated myogenesis. *Molecular and Cellular Biology*, *16*(9), 5048–5057. https://doi.org/10.1128/MCB.16.9.5048

Fu, D., Lala-Tabbert, N., Lee, H., & Wiper-Bergeron, N. (2015). Mdm2 Promotes Myogenesis through the Ubiquitination and Degradation of CCAAT/Enhancer-binding Protein β. *Journal of Biological Chemistry*, *290*(16), 10200–10207. https://doi.org/10.1074/jbc.M115.638577

Gilliam, L. A. A., & St Clair, D. K. (2011). Chemotherapy-induced weakness and fatigue in skeletal muscle: The role of oxidative stress. *Antioxidants & Redox Signaling*, *15*(9), 2543–2563. https://doi.org/10.1089/ars.2011.3965

Gollnick, P. D., Sjdin, B., Karlsson, J., Jansson, E., & Saltin, B. (1974). Human soleus muscle: A comparison of fiber composition and enzyme activities with other leg muscles. *Pflgers Archive European Journal ofPhysiology*, *348*(3), 247–255. https://doi.org/10.1007/BF00587415

Guo, C. S., Degnin, C., Fiddler, T. A., Stauffer, D., & Thayer, M. J. (2003). Regulation of MyoD Activity and Muscle Cell Differentiation by MDM2, pRb, and Sp1. *Journal of Biological Chemistry*, *278*(25), 22615–22622. https://doi.org/10.1074/jbc.M301943200

Hamid, T., Xu, Y., Ismahil, M. A., Rokosh, G., Jinno, M., Zhou, G., Wang, Q., & Prabhu, S. D. (2022). Cardiac Mesenchymal Stem Cells Promote Fibrosis and Remodeling in Heart Failure: Role of PDGF Signaling. *JACC: Basic to Translational Science*. https://doi.org/10.1016/j.jacbts.2022.01.004

Hartman, A., Bos, C. van den, Stijnen, T., & Pieters, R. (2008). Decrease in peripheral muscle strength and ankle dorsiflexion as long-term side effects of treatment for childhood cancer. *Pediatric Blood & Cancer*, *50*(4), 833–837. https://doi.org/10.1002/pbc.21325

Hawke, T. J., & Garry, D. J. (2001). Myogenic satellite cells: Physiology to molecular biology. *Journal of Applied Physiology*, *91*(2), 534–551. https://doi.org/10.1152/jappl.2001.91.2.534

Heldin, C.-H. (2013). Targeting the PDGF signaling pathway in tumor treatment. *Cell Communication and Signaling: CCS*, *11*, 97. https://doi.org/10.1186/1478-811X-11-97

Hennig, C. Cran-package fpc. Https://cran.rproject.org/web/packages/fpc/index.html. (n.d.).

Hikida, R. S., Walsh, S., Barylski, N., Campos, G., C, F., & Staron, R. S. (1998). *Is hypertrophy limited in elderly muscle fibers? A comparison of elderly and young strength-trained men. Basic Appl Myol 8*.

Hoffman, M. C., Mulrooney, D. A., Steinberger, J., Lee, J., Baker, K. S., & Ness, K. K. (2013). Deficits in Physical Function Among Young Childhood Cancer Survivors. *Journal of Clinical Oncology*, *31*(22), 2799–2805. https://doi.org/10.1200/JCO.2012.47.8081

Horn, A., Palumbo, K., Cordazzo, C., Dees, C., Akhmetshina, A., Tomcik, M., Zerr, P., Avouac, J., Gusinde, J., Zwerina, J., Roudaut, H., Traiffort, E., Ruat, M., Distler, O., Schett, G., & Distler, J. H. W. (2012). Hedgehog signaling controls fibroblast

activation and tissue fibrosis in systemic sclerosis. *Arthritis and Rheumatism*, *64*(8), 2724–2733. https://doi.org/10.1002/art.34444

Huh, M. S., Young, K. G., Yan, K., Price-O'Dea, T., & Picketts, D. J. (2017). Recovery from impaired muscle growth arises from prolonged postnatal accretion of myonuclei in Atrx mutant mice. *PLOS ONE*, *12*(11), e0186989. https://doi.org/10.1371/journal.pone.0186989

Ihalainen, J. K., Ahtiainen, J. P., Walker, S., Paulsen, G., Selänne, H., Hämäläinen, M., Moilanen, E., Peltonen, H., & Mero, A. A. (2017). Resistance training status modifies inflammatory response to explosive and hypertrophic resistance exercise bouts. *Journal of Physiology and Biochemistry*, *73*(4), 595–604. https://doi.org/10.1007/s13105-017-0590-0

Irwin, M. L., Crumley, D., McTiernan, A., Bernstein, L., Baumgartner, R., Gilliland, F. D., Kriska, A., & Ballard-Barbash, R. (2003). Physical activity levels before and after a diagnosis of breast carcinoma: The Health, Eating, Activity, and Lifestyle (HEAL) study. *Cancer*, *97*(7), 1746–1757. https://doi.org/10.1002/cncr.11227

Järvelä, L. S., Niinikoski, H., Lähteenmäki, P. M., Heinonen, O. J., Kapanen, J., Arola, M., & Kemppainen, J. (2010). Physical activity and fitness in adolescent and young adult longterm survivors of childhood acute lymphoblastic leukaemia. *Journal of Cancer Survivorship*, *4*(4), 339–345. https://doi.org/10.1007/s11764-010-0131-0

Jenney, M. E. M., Faragher, E. B., Jones, P. H. M., & Woodcock, A. (1995). Lung function and exercise capacity in survivors of childhood leukaemia. *Medical and Pediatric Oncology*, *24*(4), 222–230. https://doi.org/10.1002/mpo.2950240403

Joe, A. W. B., Yi, L., Natarajan, A., Le Grand, F., So, L., Wang, J., Rudnicki, M. A., & Rossi, F. M. V. (2010). Muscle injury activates resident fibro/adipogenic progenitors that facilitate myogenesis. *Nature Cell Biology*, *12*(2), 153–163. https://doi.org/10.1038/ncb2015

Kadi, F., Schjerling, P., Andersen, L. L., Charifi, N., Madsen, J. L., Christensen, L. R., & Andersen, J. L. (2004). The effects of heavy resistance training and detraining on satellite cells in human skeletal muscles. *The Journal of Physiology*, *558*(3), 1005–1012. https://doi.org/10.1113/jphysiol.2004.065904

Kadi, F., & Thornell, L.-E. (2000). Concomitant increases in myonuclear and satellite cell content in female trapezius muscle following strength training. *Histochemistry and Cell Biology*, *113*(2), 99–103. https://doi.org/10.1007/s004180050012

Kallenbach, J. G., Bachman, J. F., Paris, N. D., Blanc, R. S., O'Connor, T., Furati, E., Williams, J. P., & Chakkalakal, J. V. (2022). Muscle-specific functional deficits and lifelong fibrosis in response to paediatric radiotherapy and tumour elimination. *Journal of Cachexia, Sarcopenia and Muscle*, *13*(1), 296–310. https://doi.org/10.1002/jcsm.12902

Kamel, F. H., Basha, M. A., Alsharidah, A. S., & Salama, A. B. (2020). Resistance Training Impact on Mobility, Muscle Strength and Lean Mass in Pancreatic Cancer Cachexia: A Randomized Controlled Trial. *Clinical Rehabilitation*, *34*(11), 1391–1399. https://doi.org/10.1177/0269215520941912

Kaneshige, A., Kaji, T., Zhang, L., Saito, H., Nakamura, A., Kurosawa, T., Ikemoto-Uezumi, M., Tsujikawa, K., Seno, S., Hori, M., Saito, Y., Matozaki, T., Maehara, K., Ohkawa, Y., Potente, M., Watanabe, S., Braun, T., Uezumi, A., & Fukada, S.-I. (2022). Relayed signaling between mesenchymal progenitors and muscle stem

cells ensures adaptive stem cell response to increased mechanical load. *Cell Stem Cell*, *29*(2), 265-280.e6. https://doi.org/10.1016/j.stem.2021.11.003

Kendall, R. T., & Feghali-Bostwick, C. A. (2014). Fibroblasts in fibrosis: Novel roles and mediators. *Frontiers in Pharmacology*, *5*, 123. https://doi.org/10.3389/fphar.2014.00123

Khamoui, A. V., Park, B.-S., Kim, D.-H., Yeh, M.-C., Oh, S.-L., Elam, M. L., Jo, E., Arjmandi, B. H., Salazar, G., Grant, S. C., Contreras, R. J., Lee, W. J., & Kim, J.-S. (2016). Aerobic and resistance training dependent skeletal muscle plasticity in the colon-26 murine model of cancer cachexia. *Metabolism*, *65*(5), 685–698. https://doi.org/10.1016/j.metabol.2016.01.014

Kim, J. H., Jenrow, K. A., & Brown, S. L. (2014). Mechanisms of radiation-induced normal tissue toxicity and implications for future clinical trials. *Radiation Oncology Journal*, *32*(3), 103–115. https://doi.org/10.3857/roj.2014.32.3.103

Kleinerman, R. A., Boice, J. D., Storm, H. H., Sparen, P., Andersen, A., Pukkala, E., Lynch, C. F., Hankey, B. F., & Flannery, J. T. (1995). Second primary cancer after treatment for cervical cancer. An international cancer registries study. *Cancer*, *76*(3), 442–452. https://doi.org/10.1002/1097-0142(19950801)76:3<442::AID-CNCR2820760315>3.0.CO;2-L

Koeppel, M., Mathis, K., Schmitz, K. H., & Wiskemann, J. (2021). Muscle hypertrophy in cancer patients and survivors via strength training. A meta-analysis and meta-regression. *Critical Reviews in Oncology/Hematology*, *163*, 103371. https://doi.org/10.1016/j.critrevonc.2021.103371

Lam, T., Cheema, B., Hayden, A., Lord, S. R., Gurney, H., Gounden, S., Reddy, N., Shahidipour, H., Read, S., Stone, G., McLean, M., & Birzniece, V. (2020). Androgen deprivation in prostate cancer: Benefits of home-based resistance training. *Sports Medicine - Open*, *6*(1), 59. https://doi.org/10.1186/s40798-020-00288-1

Lazure, F., Farouni, R., Sahinyan, K., Blackburn, D. M., Hernández-Corchado, A., Perron, G., Ragoussis, J., Crist, C., Perkins, T. J., Jahani-Asl, A., Najafabadi, H. S., & Soleimani, V. D. (2021). Transcriptional Reprogramming of Skeletal Muscle Stem Cells by the Niche Environment. *BioRxiv*, 2021.05.25.445621. https://doi.org/10.1101/2021.05.25.445621

Lemos, D. R., Babaeijandaghi, F., Low, M., Chang, C.-K., Lee, S. T., Fiore, D., Zhang, R.-H., Natarajan, A., Nedospasov, S. A., & Rossi, F. M. V. (2015). Nilotinib reduces muscle fibrosis in chronic muscle injury by promoting TNF-mediated apoptosis of fibro/adipogenic progenitors. *Nature Medicine*, *21*(7), 786–794. https://doi.org/10.1038/nm.3869

Lepper, C., Partridge, T. A., & Fan, C.-M. (2011). An absolute requirement for Pax7-positive satellite cells in acute injury-induced skeletal muscle regeneration. *Development (Cambridge, England)*, *138*(17), 3639–3646. https://doi.org/10.1242/dev.067595

Lexell, J., Michael Sjöström, Nordlund, A., & Taylor, C. C. (1992). Growth and development of human muscle: A quantitative morphological study of whole vastus lateralis from childhood to adult age. *Muscle & Nerve*, *15*(3), 404–409. https://doi.org/10.1002/mus.880150323

Lian, X., Bond, J. S., Bharathy, N., Boudko, S. P., Pokidysheva, E., Shern, J. F., Lathara, M., Sasaki, T., Settelmeyer, T., Cleary, M. M., Bajwa, A., Srinivasa, G., Hartley, C. P., Bächinger, H. P., Mansoor, A., Gultekin, S. H., Berlow, N. E., & Keller, C. (2021). Defining the Extracellular Matrix of Rhabdomyosarcoma. *Frontiers in Oncology*, *11*, 601957. https://doi.org/10.3389/fonc.2021.601957

Lorimore, S. A., Coates, P. J., & Wright, E. G. (2003). Radiation-induced genomic instability and bystander effects: Inter-related nontargeted effects of exposure to ionizing radiation. *Oncogene*, *22*(45), 7058–7069. https://doi.org/10.1038/sj.onc.1207044

Lowe, D. A., & Alway, S. E. (2002). Animal models for inducing muscle hypertrophy: Are they relevant for clinical applications in humans? *Journal of Orthopaedic & Sports Physical Therapy*, *32*(2), 36–43.

Mashinchian, O., Pisconti, A., Le Moal, E., & Bentzinger, C. F. (2018). The Muscle Stem Cell Niche in Health and Disease. *Current Topics in Developmental Biology*, *126*, 23–65. https://doi.org/10.1016/bs.ctdb.2017.08.003

Mattusch, F., Dufaux, B., Heine, O., Mertens, I., & Rost, R. (2000). Reduction of the plasma concentration of C-reactive protein following nine months of endurance training. *International Journal of Sports Medicine*, *21*(1), 21–24. https://doi.org/10.1055/s-2000-8852

Mauro, A. (1961). SATELLITE CELL OF SKELETAL MUSCLE FIBERS. *The Journal of Biophysical and Biochemical Cytology*, *9*(2), 493–495. https://doi.org/10.1083/jcb.9.2.493

McCarthy, J. J., Mula, J., Miyazaki, M., Erfani, R., Garrison, K., Farooqui, A. B., Srikuea, R., Lawson, B. A., Grimes, B., Keller, C., Van Zant, G., Campbell, K. S., Esser, K.

A., Dupont-Versteegden, E. E., & Peterson, C. A. (2011). Effective fiber hypertrophy in satellite cell-depleted skeletal muscle. *Development*, *138*(17), 3657–3666. https://doi.org/10.1242/dev.068858

McKay, B. R., Ogborn, D. I., Baker, J. M., Toth, K. G., Tarnopolsky, M. A., & Parise, G. (2013). Elevated SOCS3 and altered IL-6 signaling is associated with age-related human muscle stem cell dysfunction. *American Journal of Physiology-Cell Physiology*, *304*(8), C717–C728. https://doi.org/10.1152/ajpcell.00305.2012

Meadors, J. L., Cui, Y., Chen, Q.-R., Song, Y. K., Khan, J., Merlino, G., Tsokos, M., Orentas, R. J., & Mackall, C. L. (2011). Murine rhabdomyosarcoma is immunogenic and responsive to Tcell-based immunotherapy. *Pediatric Blood & Cancer*, *57*(6), 921–929. https://doi.org/10.1002/pbc.23048

Murach, K. A., White, S. H., Wen, Y., Ho, A., Dupont-Versteegden, E. E., McCarthy, J. J., & Peterson, C. A. (2017). Differential requirement for satellite cells during overload-induced muscle hypertrophy in growing versus mature mice. *Skeletal Muscle*, *7*(1), 14. https://doi.org/10.1186/s13395-017-0132-z

Nederveen, J. P., Snijders, T., Joanisse, S., Wavell, C. G., Mitchell, C. J., Johnston, L. M., Baker, S. K., Phillips, S. M., & Parise, G. (2017). Altered muscle satellite cell activation following 16 wk of resistance training in young men. *American Journal of Physiology-Regulatory, Integrative and Comparative Physiology*, *312*(1), R85–R92. https://doi.org/10.1152/ajpregu.00221.2016

O'Connor, T. N., Kallenbach, J. G., Orciuoli, H. M., Paris, N. D., Bachman, J. F., Johnston, C. J., Hernady, E., Williams, J. P., Dirksen, R. T., & Chakkalakal, J. V. (2022). Endurance exercise attenuates juvenile irradiation-induced skeletal

muscle functional decline and mitochondrial stress. *Skeletal Muscle*, *12*(1), 8. https://doi.org/10.1186/s13395-022-00291-y

Otis, J. S., Lees, S. J., & Williams, J. H. (2007). Functional overload attenuates plantaris atrophy in tumor-bearing rats. *BMC Cancer*, *7*(1), 146. https://doi.org/10.1186/1471-2407-7-146

Pallafacchina, G., François, S., Regnault, B., Czarny, B., Dive, V., Cumano, A., Montarras, D., & Buckingham, M. (2010). An adult tissue-specific stem cell in its niche: A gene profiling analysis of in vivo quiescent and activated muscle satellite cells. *Stem Cell Research*, *4*(2), 77–91.

Paris, N. D., Kallenbach, J. G., Bachman, J. F., Blanc, R. S., Johnston, C. J., Hernady, E., Williams, J. P., & Chakkalakal, J. V. (2020). Chemoradiation impairs myofiber hypertrophic growth in a pediatric tumor model. *Scientific Reports*, *10*(1), 19501. https://doi.org/10.1038/s41598-020-75913-w

Patsalos, A., Pap, A., Varga, T., Trencsenyi, G., Contreras, G. A., Garai, I., Papp, Z., Dezso, B., Pintye, E., & Nagy, L. (2017). In situ macrophage phenotypic transition is affected by altered cellular composition prior to acute sterile muscle injury. *The Journal of Physiology*, *595*(17), 5815–5842. https://doi.org/10.1113/JP274361

Paulino, A. C. (2004). Late effects of radiotherapy for pediatric extremity sarcomas. *International Journal of Radiation Oncology, Biology, Physics*, *60*(1), 265–274. https://doi.org/10.1016/j.ijrobp.2004.02.001

Peck, B. D., Murach, K. A., Walton, R. G., Simmons, A. J., Long, D. E., Kosmac, K., Dungan, C. M., Kern, P. A., Bamman, M. M., & Peterson, C. A. (2022). A muscle cell-macrophage axis involving matrix metalloproteinase 14 facilitates

extracellular matrix remodeling with mechanical loading. *FASEB Journal: Official Publication of the Federation of American Societies for Experimental Biology*, *36*(2), e22155. https://doi.org/10.1096/fj.202100182RR

Radbruch, L., Elsner, F., Trottenberg, P., Strasser, F., & Fearon, K. (2010). Clinical practice guidelines on cancer cachexia in advanced cancer patients. *Aachen: Department of Palliative Medicinen/European Palliative Care Research Collaborative*.

Rogers, L. Q., Courneya, K. S., Robbins, K. T., Malone, J., Seiz, A., Koch, L., & Rao, K. (2008). Physical activity correlates and barriers in head and neck cancer patients. *Supportive Care in Cancer*, *16*(1), 19–27. https://doi.org/10.1007/s00520-007-0293-0

Rogers, L. Q., Courneya, K. S., Robbins, K. T., Malone, J., Seiz, A., Koch, L., Rao, K., & Nagarkar, M. (2006). Physical activity and quality of life in head and neck cancer survivors. *Supportive Care in Cancer*, *14*(10), 1012–1019. https://doi.org/10.1007/s00520-006-0044-7

Rosenblatt, J. D., & Parry, D. J. (1992). Gamma irradiation prevents compensatory hypertrophy of overloaded mouse extensor digitorum longus muscle. *Journal of Applied Physiology*, *73*(6), 2538–2543. https://doi.org/10.1152/jappl.1992.73.6.2538

Rossi, S., Stoppani, E., Puri, P. L., & Fanzani, A. (2011). Differentiation of human rhabdomyosarcoma RD cells is regulated by reciprocal, functional interactions between myostatin, p38 and extracellular regulated kinase signalling pathways.

European Journal of Cancer, *47*(7), 1095–1105. https://doi.org/10.1016/j.ejca.2010.12.010

Roubos, S., D'Souza, D., Hernández-Saavedra, D., Xu, G., Collao, N., Emmons, R., Larkin, J., Lloyd, J., Vanhie, J. J., Pan, Y.-X., Chen, H., & De Lisio, M. (2021). Weight loss with exercise improves muscle architecture and progenitor cell populations compared with weight loss alone in mice with preneoplastic colorectal lesions. *Applied Physiology, Nutrition, and Metabolism*, *46*(7), 837–845. https://doi.org/10.1139/apnm-2020-0956

Roy et al. (1999). Modulation of myonuclear number in functionally overloaded and exercised rat plantaris fibers | Journal of Applied Physiology. *Journal of Applied Physiology*, *87*(2), 634– 642.

Saito, Y., Chikenji, T. S., Matsumura, T., Nakano, M., & Fujimiya, M. (2020). Exercise enhances skeletal muscle regeneration by promoting senescence in fibro-adipogenic progenitors. *Nature Communications*, *11*(1), 889. https://doi.org/10.1038/s41467-020-14734-x

Sambasivan, R., Yao, R., Kissenpfennig, A., Van Wittenberghe, L., Paldi, A., Gayraud-Morel, B., Guenou, H., Malissen, B., Tajbakhsh, S., & Galy, A. (2011). Pax7-expressing satellite cells are indispensable for adult skeletal muscle regeneration. *Development (Cambridge, England)*, *138*(17), 3647–3656. https://doi.org/10.1242/dev.067587

Santini, M. P., Malide, D., Hoffman, G., Pandey, G., D'Escamard, V., Nomura-Kitabayashi, A., Rovira, I., Kataoka, H., Ochando, J., Harvey, R. P., Finkel, T., & Kovacic, J. C. (2020). TissueResident PDGFRα+ Progenitor Cells Contribute to Fibrosis versus Healing in a Context- and Spatiotemporally Dependent

Manner. *Cell Reports*, *30*(2), 555-570.e7. https://doi.org/10.1016/j.celrep.2019.12.045

Sawano, S., Komiya, Y., Ichitsubo, R., Ohkawa, Y., Nakamura, M., Tatsumi, R., Ikeuchi, Y., & Mizunoya, W. (2016). A One-Step Immunostaining Method to Visualize Rodent Muscle Fiber Type within a Single Specimen. *PLOS ONE*, *11*(11), e0166080. https://doi.org/10.1371/journal.pone.0166080

Scaramozza, A., Park, D., Kollu, S., Beerman, I., Sun, X., Rossi, D. J., Lin, C. P., Scadden, D. T., Crist, C., & Brack, A. S. (2019). Lineage Tracing Reveals a Subset of Reserve Muscle Stem Cells Capable of Clonal Expansion under Stress. *Cell Stem Cell*, *24*(6), 944-957.e5. https://doi.org/10.1016/j.stem.2019.03.020

Scheede-Bergdahl, C., & Jagoe, R. T. (2013). After the chemotherapy: Potential mechanisms for chemotherapy-induced delayed skeletal muscle dysfunction in survivors of acute lymphoblastic leukaemia in childhood. *Frontiers in Pharmacology*, *4*. https://doi.org/10.3389/fphar.2013.00049

Seale, P., Asakura, A., & Rudnicki, M. A. (2001). The Potential of Muscle Stem Cells. *Developmental Cell*, *1*(3), 333–342. https://doi.org/10.1016/S1534-5807(01)00049-1

Segal, R. J., Reid, R. D., Courneya, K. S., Sigal, R. J., Kenny, G. P., Prud'Homme, D. G., Malone, S. C., Wells, G. A., Scott, C. G., & Slovinec D'Angelo, M. E. (2009). Randomized Controlled Trial of Resistance or Aerobic Exercise in Men Receiving Radiation Therapy for Prostate Cancer. *Journal of Clinical Oncology*, *27*(3), 344–351. https://doi.org/10.1200/JCO.2007.15.4963

Siegel, R. L., Miller, K. D., & Jemal, A. (2020). Cancer statistics, 2020. *CA: A Cancer Journal for Clinicians*, *70*(1), 7–30. https://doi.org/10.3322/caac.21590

Soffe, Z., Radley-Crabb, H. G., McMahon, C., Grounds, M. D., & Shavlakadze, T. (2016). Effects of loaded voluntary wheel exercise on performance and muscle hypertrophy in young and old male C 57 B l/6 J mice. *Scandinavian Journal of Medicine & Science in Sports*, *26*(2), 172–188.

Sousa-Victor, P., García-Prat, L., & Muñoz-Cánoves, P. (2022). Control of satellite cell function in muscle regeneration and its disruption in ageing. *Nature Reviews. Molecular Cell Biology*, *23*(3), 204–226. https://doi.org/10.1038/s41580-021-00421-2

St. Jude Children's Research Hospital. (2016). *Childhood Cancer Survivor Study, Baseline Data*. www.stjude.org/ccss Straub, J. M., New, J., Hamilton, C. D., Lominska, C., Shnayder, Y., & Thomas, S. M. (2015). Radiation-induced fibrosis: Mechanisms and implications for therapy. *Journal of Cancer Research and Clinical Oncology*, *141*(11), 1985–1994. https://doi.org/10.1007/s00432015-1974-6

Stubblefield, M. D. (2011). Radiation fibrosis syndrome: Neuromuscular and musculoskeletal complications in cancer survivors. *PM & R: The Journal of Injury, Function, and Rehabilitation*, *3*(11), 1041–1054. https://doi.org/10.1016/j.pmrj.2011.08.535

Sun, X., Guo, W., Shen, J. K., Mankin, H. J., Hornicek, F. J., & Duan, Z. (2015). Rhabdomyosarcoma: Advances in molecular and cellular biology. *Sarcoma*, *2015*.

Theret, M., Rossi, F. M. V., & Contreras, O. (2021). Evolving Roles of Muscle-Resident FibroAdipogenic Progenitors in Health, Regeneration, Neuromuscular Disorders, and Aging. *Frontiers in Physiology*, *12*, 673404. https://doi.org/10.3389/fphys.2021.673404

Tidball, J. G. (2017). Regulation of muscle growth and regeneration by the immune system. *Nature Reviews. Immunology*, *17*(3), 165–178. https://doi.org/10.1038/nri.2016.150

Tiffin, N., Williams, R. D., Shipley, J., & Pritchard-Jones, K. (2003). PAX7 expression in embryonal rhabdomyosarcoma suggests an origin in muscle satellite cells. *British Journal of Cancer*, *89*(2), 327–332. https://doi.org/10.1038/sj.bjc.6601040

Toth, M. J., Callahan, D. M., Miller, M. S., Tourville, T. W., Hackett, S. B., Couch, M. E., & Dittus, K. (2016). Skeletal muscle fiber size and fiber type distribution in human cancer: Effects of weight loss and relationship to physical function. *Clinical Nutrition (Edinburgh, Scotland)*, *35*(6), 1359–1365. https://doi.org/10.1016/j.clnu.2016.02.016

Ueha, S., Shand, F. H., & Matsushima, K. (2012). Cellular and molecular mechanisms of chronic inflammation-associated organ fibrosis. *Frontiers in Immunology*, *3*, 71.

Uezumi, A., Fukada, S., Yamamoto, N., Takeda, S., & Tsuchida, K. (2010). Mesenchymal progenitors distinct from satellite cells contribute to ectopic fat cell formation in skeletal muscle. *Nature Cell Biology*, *12*(2), 143–152.

Uezumi, A., Ito, T., Morikawa, D., Shimizu, N., Yoneda, T., Segawa, M., Yamaguchi, M., Ogawa, R., Matev, M. M., & Miyagoe-Suzuki, Y. (2011). Fibrosis and

adipogenesis originate from a common mesenchymal progenitor in skeletal muscle. *Journal of Cell Science*, *124*(21), 3654–3664.

Valero, M. C., Huntsman, H. D., Liu, J., Zou, K., & Boppart, M. D. (2012). Eccentric exercise facilitates mesenchymal stem cell appearance in skeletal muscle. *PloS One*, *7*(1), e29760. https://doi.org/10.1371/journal.pone.0029760

Valle-Tenney, R., Rebolledo, D., Acuña, M. J., & Brandan, E. (2020). HIF-hypoxia signaling in skeletal muscle physiology and fibrosis. *Journal of Cell Communication and Signaling*, *14*(2), 147–158. https://doi.org/10.1007/s12079-020-00553-8

Walters, Z. S., Villarejo-Balcells, B., Olmos, D., Buist, T. W., Missiaglia, E., Allen, R., Al-Lazikani, B., Garrett, M. D., Blagg, J., & Shipley, J. (2014). JARID2 is a direct target of the PAX3-FOXO1 fusion protein and inhibits myogenic differentiation of rhabdomyosarcoma cells. *Oncogene*, *33*(9), 1148–1157.

Wasti, A. T., Mandeville, H., Gatz, S., & Chisholm, J. C. (2018). Rhabdomyosarcoma. *Paediatrics and Child Health*, *28*(4), 157–163.

West, D. W. D., Burd, N. A., Churchward-Venne, T. A., Camera, D. M., Mitchell, C. J., Baker, S. K., Hawley, J. A., Coffey, V. G., & Phillips, S. M. (2012). Sex-based comparisons of myofibrillar protein synthesis after resistance exercise in the fed state. *Journal of Applied Physiology*, *112*(11), 1805–1813. https://doi.org/10.1152/japplphysiol.00170.2012

White, Z., Terrill, J., White, R. B., McMahon, C., Sheard, P., Grounds, M. D., & Shavlakadze, T. (2016). Voluntary resistance wheel exercise from mid-life prevents sarcopenia and increases markers of mitochondrial function and

autophagy in muscles of old male and female C57BL/6J mice. *Skeletal Muscle*, *6*(1), 1–21.

Williams, J. P., Calvi, L., Chakkalakal, J. V., Finkelstein, J. N., O'Banion, M. K., & Puzas, E. (2016). Addressing the Symptoms or Fixing the Problem? Developing Countermeasures against Normal Tissue Radiation Injury. *Radiation Research*, *186*(1), 1–16. https://doi.org/10.1667/RR14473.1

Wosczyna, M. N., Konishi, C. T., Perez Carbajal, E. E., Wang, T. T., Walsh, R. A., Gan, Q., Wagner, M. W., & Rando, T. A. (2019). Mesenchymal Stromal Cells Are Required for Regeneration and Homeostatic Maintenance of Skeletal Muscle. *Cell Reports*, *27*(7), 2029-2035.e5. https://doi.org/10.1016/j.celrep.2019.04.074

Wosczyna, M. N., & Rando, T. A. (2018). A muscle stem cell support group: Coordinated cellular responses in muscle regeneration. *Developmental Cell*, *46*(2), 135–143.

Yin, H., Price, F., & Rudnicki, M. A. (2013). Satellite cells and the muscle stem cell niche. *Physiological Reviews*, *93*(1), 23–67.

Yoon, M.-S. (2017). MTOR as a Key Regulator in Maintaining Skeletal Muscle Mass. *Frontiers in Physiology*, *8*, 788. https://doi.org/10.3389/fphys.2017.00788

Zhang, M., Truscott, J., & Davie, J. (2013). Loss of MEF2D expression inhibits differentiation and contributes to oncogenesis in rhabdomyosarcoma cells. *Molecular Cancer*, *12*(1), 1–14.

Zhang, Q., Joshi, S. K., Lovett, D. H., Zhang, B., Bodine, S., Kim, H. T., & Liu, X. (2014). Matrix metalloproteinase-2 plays a critical role in overload induced skeletal muscle hypertrophy. *Muscles, Ligaments and Tendons Journal*, *4*(4), 446–454.

Zou, K., Huntsman, H. D., VALERO, C. M., Adams, J., Skelton, J., De Lisio, M., Jensen, T., & Boppart, M. D. (2015). Mesenchymal stem cells augment the adaptive response to eccentric exercise. *Medicine & Science in Sports & Exercise*, *47*(2), 315–325.

Appendix A – Behavioural Testing

Forelimb Grip Strength

Day of Testing

SETUP

1. Bring your mice to the testing room and leave to habituate for 30-60 minutes.

- Turn over the “Do Not Disturb” sign hanging outside of the door to ensure that no one will enter during testing.

BEGIN TESTING

1. Always weigh each mouse before taking grip strength measurements, as grip data can be normalized using animal body weight.
2. Press the power button to turn on the instrument.

- The instrument is ready to use when a numerical value is displayed on the screen.

3. Press the Zero key to reset the value to 0.
4. Hold the mouse (see below for holding techniques) and gently move it close to the grid

   until the mouse grabs it with its front paws. Gently pull the mouse along a horizontal plane relative to the grid at a steady speed of ~ 2.5 cm/sec, until the animal releases the grid.

- Pulling the mice away more slowly results in many mice prematurely releasing the bar with one or both paws.

5. Record the value of force that is displayed on the screen in gram force (GF).

- The instrument only displays the maximal value.

6. Press the Zero key to clear the screen.

- You may have to press it multiple times.

7. Repeat for a maximum of 8 consecutive measurements for one animal.

- Allow mice to rest for roughly 10 seconds between trials.

8. Place the mouse back in its home cage.

9. Repeat for all mice.

10. When finished, log off the computer, return the mice to their regular housing room, and clean the testing room.

Endurance Testing

1. Prior to starting the test, mice will be habituated to the testing room for 30 minutes

2. They will then be placed on the treadmill, one mouse per lane

3. Testing will begin at a speed of 11 m/min and increased by 1 m/min every 2 minutes

4. Bristles of a paint brush will be used to motivate the mice to continue to run

5. A mouse was considered to have completed the test if it:

    a. was resistant to stimulation
    b. remained on the platform for longer than two minutes or

    c. stayed approximately one body length away from the platform for longer than five continuous seconds

6. The speed and time at which each mouse finished the test will be documented

Appendix B – EchoMRI Set-Up and Protocol

SETUP

- Log on to the computer.
- Open the Echo software program on the desktop.
- Select Folder > Browse/New and choose the appropriate experimental folder.
- If creating a new folder, it must be located within the EchoScans folder.
- Select the species (Mice) from the drop-down list on the right hand side of the screen.
- Set the Primary Accumulation to 1.
- Set Water Stage to No.
- System Test
- Insert the test probe with the oil-filled bottle into the MRI. Put the shorter end in first, then push it in as far as possible.
- Select System Test > Yes. When finished, you will see System Test Completed Successfully.
- Run a system test at the beginning of every experiment.
- If the test was not successful, the machine will automatically calibrate itself and re-run the system test.

To begin testing:

- Place the animal in the appropriately sized red plastic tube (maximum weights are printed on the tubes; for mice, a size 40 tube is acceptable for mice 20-60g).
- Place the animal into the open end of the tube. If you are having difficulties getting a mouse into the tube, hold the tube horizontally and hold the mouse by the base of its tail near the opening of the tube to encourage hiding behavior.
- Gently push the animal to the end of the tube with the plastic insert.
- Leave enough space for the length of the animal's body, not including the tail.
- Ensure the animal is NOT compressed in the tube. Too little space can result in suffocation. It is better to give the animal too much space than too little as animal movement will not affect EchoMRI readings.
- Use the Velcro to lock the insert in place.
- Place the tube inside the machine, with the end of the tube holding the animal going in first. Push the tube in as far as possible, being careful not to push the insert and injure the animal.
- Select Start Scan.
- Input the mouse ID (and any other data/comments) in the dialog box.
- These can be added or edited later if necessary.
- NOTE: the placement of the plastic insert CAN NOT be adjusted while the tube is inside the machine. The tube MUST be removed from the machine and the mouse fully visible in the tube for any adjustments to the placement of the plastic insert to be made.
- After testing is complete you will see Scan ALL DONE in the dialog box.

- Each scan takes approximately two minutes, meaning the mouse will spend less than three minutes in the test tube. Do not leave the mouse in the sample tube for more than five minutes – if issues arise place the mouse back into it's cage and call for assistance.
- Remove the mouse from the machine and place it back in it's cage
- Clean out the tube after each mouse
- Repeat for each mouse.

To export your data:

- Highlight each trial from the list
- Select Review > Extract Table.
- Choose the destination folder and name the file.

Appendix C - RMS Injection and Therapy Protocol

RMS Injection

- Culture RMS M3-9-M cells in 3-5 10 cm plates until appx. 80% confluent.
    - o Note these cells will reach confluency extremely quickly.
- Cells should be cultured in specific RMS media consisting of RPMI 1640 and 1% L-glutamine with and added 10% heat-inactivated fetal bovine serum, HEPES buffer, 1% non-essential amino acids, 1% sodium pyruvate, 1% penicillin/streptomycin, and 50 mM 2mercaptoethanol.
- Lift cells from plate using trypsin and centrifuge – remove cell debris in supernatant and re-suspend in sterile PBS.
- Using the cells counter – count the number of cells per ml of solution.
- Resuspend cells with more PBS accordingly so that you can accurately inject 100,000 cells into each mouse (should be appx 10ul per 100,000 cells)
- This should be performed the morning of injections.
- Using isofluorane sedate each mouse and remove hair on the entire left hindlimb using clippers to ensure accurate location of the RMS injection
- Using a sterile insulin syringe – inject the M3-9-M cells into both lobes of the left GAS hindlimb of each mouse.
- After each injection carefully place mouse back into its individual cage and check to make sure that it recovers well after the sedation
- Leave mice to recover for 3 days without manipulation – but continue health inspections

    daily

Chemotherapy Administration

- Dissolve solid vincristine sulfate (Sigma Aldrich, cat#. V8388) in sterile water and ensure it is homogenously combined to a concentration of 20mg/ml
- This solution can be stored in the -20c freezer for a few weeks and it is suggested to prepare this stock solution before required, and diluting it to the appropriate concentration the day of the vincristine injections
- Freshly dilute this stock solution the morning of injection to a concentration of 0.2mg/ml (1:100) in PBS
- To ensure that each dosage is specific for each individual mouse, weigh each mouse using an electronic scale the day of the injections and calculate the dosage using this body weight
    - It is important to weigh each mouse to ensure they are >12g at time of vincristine administration as a lower weight may be fatal
- Ensure that each mouse receives 1mg/kg of body weight (5ul per gram)
- Inject each mouse I.P. using a sterile standard insulin syringe
- Monitor the mice closely for the next days during health checks before proceeding to radiation

Fractionated Radiation

- The morning of each mouse radiation dosage ensure that you arrive early to turn on the X-RAD 320 and give it time to warm up
- Ensure that the correct filter is placed into the machine (animals, not cells)
- Bring the individual cages in carts to the machine when ready to acclimatize to the x-ray room for 30mins

- Using isofluorane sedate the mouse in its cage, then quickly attach the isofluorane machine to the back of the irradiator using the correct connection tube (this will allow you to use the nose cone in the irradiator to ensure that the mouse stays sedated the entire time you irradiate
- Gently remove the sedated mouse from it cage and position it with it's nose in the actively pumping nose cone inside the irradiator and ensure that the beam of light (signalling the area that the radiation will be applied) is fully covering the area you wish to irradiate
- Extend the left leg of the mouse outward and gently tape with skin-safe medical tape

- Place the lead body shield over the mouse with the left leg sticking out and ensure that no other body parts of the mouse are exposed to the radiation beam
- Close the X-RAD door gently and ensure it doesn't slam

- Convert 4.8Gy to the appropriate MU dosage using the conversion chart on the radiator (double check to make sure you have the right dose and write it down on a sticky to make sure you administer that same dose to each mouse)
- Then hit enter to confirm the dose selection

- Hit start to begin the radiation process and step out of the room
- After the radiation has finished, the light will go off and you can gently remove the mouse and put it back in it's cage
- Monitor the mouse after to make sure it has no issues waking up from the sedation

- After all doses have been administered, move each mouse to a sterile cage to prevent infection and monitor closely for the next week to ensure no recurrence of tumor

Appendix D - RET set-up, Monitoring, and Wheel Data Analysis

1) Reserve 10 low-profile wireless running wheels (ENV-044 and ENV-047) from the behavioural core
2) Place batteries into the bottom of the wheels

3) Wheel the cart with the monitoring software – “Wheel Manager Software SOF-860” into the room where the mice are housed.
4) to ensure that the software is picking up the wheels – you can look to see if every wheel is coming up on the screen (each wheel has a specific number)
5) Move the bedding at the bottom of each cage to ensure a smooth surface

6) Place the docking plate at the bottom of the cage and ensure that there are no pellets between the dock and the floor of the cage
7) Make sure the 2 pegs on the dock are sticking up and fit the low-profile wheel securely onto the dock
8) Hot glue a 1g magnet (K&J magnetics) to the perimeter of the wheel as close as you can to the outside to ensure maximal resistance.
9) After the original magnet is securely attached, all other incremental additions of weight can be added simply by allowing the strong attractive forces between magnets to keep them on
10) The software will count total revolutions for a given time period which you can set to 24 hours
11) Come in everyday to ensure that the software is picking up the number of revolutions each mouse is completing and export the total revolutions for each day in the form of an excel sheet (you will want to complete this every day in case a wheel goes offline during the night, or there is a power outage, and the computer stops working)

12) To export data to a excel file, select file → export sensor data.

13) The export data pop-up will appear – make sure include sensor headings, include row labels, and include columns labels are all selected
14) Under report format select ‘date/time column’

15) Under activity units select ‘revolutions

16) Edit the ‘output file’ at the bottom of the screen to save this file to a specific place – and the press the ‘ok’ button
17) Each wheel has a conversion factor of 6.0198 cm for each revolution – this can be used to calculate total distance run per day

Appendix E - Mouse Necropsy

Sacrifice of Mice

1. Remove water and lid from cage and place it into the container in room 1247.

2. Remove food and bedding and dispose of both accordingly

3. Place CO2 specific metal lid onto the cage and confirm that both holes are over the opening.
4. Attach the CO2 hose to the metal lid and open the CO2 valve with 2 turns

5. Using the instructions on the metal cage - fine-tune the CO2 gauge to ensure that the proper amount of CO2 is being released for the number of cages in line (1 cage, starts at
   1.53 near the end)

6. Watch the mouse carefully – it will quicken its breath, start to stumble, and then pass out.

   Just because it has stopped moving does not confirm that it is
   deceased … ensure that blinking and breathing has stopped and
   wait 10 seconds
7. Turn the gauge down and the CO2 tank off.

8. Remove the hose and metal lid

9. Remove the mouse from the cage and implement cervical dislocation to confirm death
   a. Spread all 4 legs out on the table and palpate on the cervical vertebrae where the cervical joint is
   b. Press down firmly using the metal key card until you can feel/ hear a click

c. Corroborate the dislocation by feeling for the gap between the vertebrae
d. Place the sacrificed mouse in a black garbage bag for transportation back up to the lab

10. Clean your workstation by spraying all surfaces with ethanol and place the empty cage into the cage disposal room

Dissection of Mice

1. Prepare the hood by spraying with ethanol and ensuring all tweezers and scissors are cleaned thoroughly
2. Remove the mouse from the black plastic garbage bag and spray generously with ethanol
3. Separate one set of tweezers and scissors for removal of the skin and the other for harvesting of the muscle
4. Place the mouse belly up, pinch the skin on the belly and pull up
5. Snip the skin and avoid puncturing organs underneath
6. Once a hole has been created around the umbilical on the abdomen – cut around the circumference of the mouse and remove the bottom portion (i.e., pants) of the mouse by holding the top of the mouse (around the neck) with one hand and pulling the skin around the legs down and off the ankles
7. Once the skin is removed – turn the mouse back facing up and slide the tweezers under the Achilles tendon of the back hindlimb
8. Run the tweezers up and turn the tibia to separate the gastrocnemius from the bone and

   lift it up
9. Cut the tendon with the tweezers and pull the muscle up the back of the leg up towards the back of the knee

10. Cut as close to the back of the knee as possible to preserve the most amount of muscle

11. Cut away all accessory muscles but keep the soleus intact behind the gastrocnemius

Appendix F – Cryostat Muscle Sectioning Protocol

Materials:

- Tweezers
- Slides
- Razor blade
- Paint brushes
- OCT
- Gloves
- Chucks
- 2 slide boxes
- S35 microtome cryostat blade

Protocol:

- Take out removable pieces and clean the inside of the HM525 MX cryostat with 100% ethanol
- Place all pieces back inside the cryostat and set the temperature to -20 °C
- Gather samples from -80 °C freezer and maintain on dry ice
- Select primary sectioning widths (20µm for general sectioning of only OCT and 8-10µm for sectioning of the muscle)

- Cover holes in cryostat with tin foil to avoid losing sample and place all tools (paint brushes, tweezers, razor blade) inside the cryostat to acclimate to the temperature
- Maintain sectioning angle at 10 ° and place S35 microtome cryostat blade in position

(*note: ensure cover is always covering the blade when your hands are in the cryostat)

- Remove your sample from the dry ice and place in the cryostat – allow to adjust to -20 °C temperature for 10 minutes before mounting
- After 10 minutes, mount the sample onto the chuck using OCT and allow to solidify before orienting the chuck into the cryostat for sectioning
- Remove the cover from the S35 microtome cryostat blade and cut through the OCT at 20µm until pink of the muscle is just visible
- Switch the 10µm sectioning width for muscle sections and make sure blade is cutting flat across the centre of the muscle cross-sectionally
- Use the anti-roll plate to keep the section that you want to visualize from curling up
- Warm up the slide with your hand so that the sample sticks
- Using the paint brushes to adjust the section so that it does not roll up and lays flat
- Stick the slide to the sample and visualize under the microscope to ensure proper cross-sections of individual fibres are present
- Once contented with appearance of the section – use your final (non-practice slides) to mount your good and final sample and keep it cold in a slide box in the cryostat until you are ready to transfer back to the -80 °C freezer

Appendix G – Immunohistochemical Staining

Myosin Heavy Chain/ Laminin Stain (Adapted from NC's protocol)

Primary antibodies:

- **BA-D5** (IgG-2b) Mouse anti-myosin Heavy Chain (MHC) Type 1, DSHB
- **SC-71** (IgG1) Mouse anti-myosin Heavy Chain Type IIa, DSHB
- **BF-F3** (IgM) mouse anti-myosin Heavy Chain Type IIb DSHB
- Laminin β-2/ γ-1 Monoclonal (A5), rat anti-laminin **(MA1-06100)** (IgG), ThermoFisher

  Scientific

Secondary antibodies:

- Alexa Fluor 488 AffiniPure Goat Anti-Mouse IgG, Fcγ subclass 1 specific **(115-545-205)**, Jackson Immunoresearch lab
- Alexa Fluor 647 AffiniPure Goat Anti-Mouse IgG, Fcγ subclass 2b specific **(115-605-207)**,

  Jackson Immunoresearch lab

- Cy™3 AffiniPure Fab Fragment Goat Anti-Mouse IgM, μ chain specific
- Alexa Fluor 594 Goat Anti-rat IgG (H+L) **(A-11007)**, ThermoFisher Scientific

- Allow sections to thaw and air-dry (10-15min).
- circle sections with immunopen (front of slide).

- Line the bottom of a slide box with paper towel dampened with ddH2O, to keep a moist environment to prevent slide dehydration.
- Add 5% BSA in 1xPBS and incubate 1hr. at RT (≈21°C).
- Add laminin (MA1-06100) [1:200] in 5% G/S in 1xPBS to 1'AB sections.
    - Add 5% G/S only to the 2'AB sections.
- Incubate O/N at 4°C (16-20hrs=ideal, 24hrs. max.)
- Wash in 1 x PBS, 3 x 5 min.
- Add AF594 anti-rat (A-11007) [1:300] in 1% BSA, 1 x PBS.
- Incubate for 1hr. at RT (≈21°C). o Add mixture to both sections.
- Wash in 1 x PBS, 3 x 5 min.
- Block with M.O.M., 1h at RT (1:25 (Drops) in 1x PBS
- Wash 1xPBS 2x2min
- add M.o.M diluent 5 min (1:12.5 in 1xPBS)
- Add BA-D5 [1:100], SC-71 [1:100], and BF-F3 [1:25] in 1% BSA in 1xPBS.
- Incubate in the heated incubatcytoxor for 45min at 37°C.
    - Add 1% BSA in 1xPBS only to the 2'AB sections.
- Wash in 1 x PBS, 3 x 5 min.
- Add AF488-IgG1 [1:100], AF647-IgG-2b [1:100], and Cy3 [1:50] in 0.5% BSA, 5% G/S in

  1xPBS.

- Incubate for 1hr. at RT (≈21°C).
    - Add mixture to both sections.
- Wash in 1 x PBS, 3 x 5 min.
- Add DAPI, 1x5min.
- Wash in 1 x PBS, 3 x 2 min.
- Add fluoromount and coverslip and let dry for (10-15min).
- Be careful adding the coverslip since the sections are fragile since they are not fixed. Do not press or move the coverslip after mounting, gently drop it.
- Add nail polish around the edge of the slide and coverslip to create a seal.
- Let slides sit for at least 1hr. prior to imaging. Leaving O/N is ideal.
- Store the slides long-term at 4°C.

Appendix H – Imaging Protocols Used in Thesis

Scanning Muscle Sections for Trichrome Analysis – EVOS FL2 Microscope

Turning on the Microscope:

- Turn on all equipment (fluorescent bulb, microscope, and computer)
- Open Auto 2 program on computer, program will calibrate automatically
- Place slide in slide holder stage

Identifying the Section and Adjusting Image:

- Select the accurate slide holder and make sure it is in the correct orientation
- Set the objective to 20x (default)
- Move the stage using the arrows on the computer or touch screen for fine movement.
- Increase the brightness of the image using the brightness range.
- The initial screen may appear blue – but the image is easily brought into focus by using the ‘coarse’ focus adjustment.
- Once satisfied, capture the image using the command located below these parameters:
    - Select channel as ‘trans’ since there are no fluorescent channels to capture
    - Select ‘autofocus’ under options → set ‘every 3 fields’ for autofocus frequency

- Under locations select ‘create locations’ and create a rectangular area around your desired muscle section – once complete this should appear under scan locations
- Select the newly created rectangle and select ‘assign scan area’
- Ensure area acquisition order is ‘serpentine horizontal’ and field acquisition order is ‘spiral outward counterclockwise’
- In image save settings ensure ‘TIF’ file format is selected and ‘tiled image merged channels is selected under displayed images
- Select ‘pseudocolor’ under color and ‘tiled per location’
- You can choose the location you want to save the image under “image save settings”, and are able to adjust the file name beside ‘prefix’
- Once all parameters have been adjusted, select ‘Run’ to begin scanning the section.

- Note that the average duration of scanning is approximately 5-10 minutes.
- Scanning lots of blank space (when no muscle section is present) will significantly increase the scan time, therefore it is best to ensure the rectangular scan area is as tight to the section as possible without cutting off any of the muscle.

<u>Scanning Muscle Sections for Myosin Heavy Chain Analysis Zeiss Celldiscoverer Microscope</u>

- turn on computer and the celldiscoverer using the power button and allow it to fully calibrate
- **NB: do not open Zeiss software on the desktop before the microscope has fully configurated and the loading bar on the machine has reached the end → this may lead to problems processing the sample and extremely long scan time

- After microscope has booted, open the Zeiss software on the desktop
- Select ‘sample acquisition’
- Configure your selected experiment (select appropriate plate and run time) and select ‘run’ experiment
- It will take a few minutes for microscope to scan each slide, after it is finished the churning circle will stop
- click on ‘live’ to see a live picture of the slide
- click ‘snap’ to take a picture of the view of the microscope at a current place in time
- select the appropriate channels (DAPI, AF488, AF647, Cy3) by clicking on the ‘channels’ tab on the right side of the screen and clicking the gear icon and adding channels individually
- make sure DAPI is set as you reference channel and adjust the other one’s according to DAPI
- using coarse and fine adjustment use the mouse to toggle and zoom into the nuclei and adjust the focus so on the DAPI channel so that the nuclei become clear and that is maintained for the entire image
- select auto-exposure first and adjust each exposure for the channels accordingly that each muscle fibre colour is bright and clearly distinguishable between the other fibres. This can be done by selecting individual channels so that only the selected fibres appear and then comparing that with the other channels by including 2 together.
- Make sure the exposure for each channel is written down and applied now to each muscle section being imaged to ensure reliability and consistency in image acquisition

- Once the entire muscle on the slide is in focus create different ROIs by adding tiles
- Ensure that each tile is consistent size for all ROIs so that each ROI for each muscle is covering the same amount of area. Ensure that the size of your tile covers appx. 150 fibres
- To keep the adjusted magnification, select the gear icon by the tile bar and hit ‘set z for selected tile region’ this will make sure that your images do not lose focus
- Move this tile around the muscle at 4 distinct locations (i.e., top, bottom, right and left) to ensure an accurate representation of all fibres in the muscle and make sure that this tile placement is kept consistent for all muscle samples analyzed
- Hit start experiment to take a picture of the tile at each location
- To save to picture of the tiles select ‘processing’ from the upper menu – select ‘stitching’ and then ‘fuse tiles’
- Hit ‘apply’ and this will create a new image tab with the fused tiles
- Under graphics on the bottom pane of the image – select the ruler icon to add a scale bar (ensure the scale bar is not covering full fibres that need to be analyzed and place in a corner of the image)
- First save each image as a czi file in an appropriate czi folder so that you can re-manipulate each image if needed. Select the ‘save’ icon in the top left upper toolbar and save to the desired folder
- To save the TIFF file of that same image for analysis select ‘processing’ from the upper left
- Under method select ‘image export’
- Under ‘file type’ select Tagged Image File Format (TIFF)

- Under ‘export to’ select the folder you want to save the image to
- Under ‘prefix’ rename your image to include the name of the muscle and which ROI it is Image J Analysis - Trichrome

Steps for measuring Trichrome:

1) Install colour deconvolution plugin
2) Drag and drop image to analyze into image J
3) Adjust brightness of image, if necessary, Image→adjust→brightness/contrast
4) Deconvolute the image, Image → Colour → Colour deconvolution2
5) Select Masson Trichrome from the drop-down menu and then Press ok
6) Delete the first two red and black images and select the blue image
7) Adjust the threshold in order to select for the blue fibrotic tissue, Image → Adjust → Threshold
    a. *NB: select blue as well as purple tissue – if stain is not washed out properly it can lead to overlap in colours (threshold between 0-110 or 0-140 should account for this)
8) Select ‘apply’ threshold

a. *NB: in order for threshold to apply circle a portion of the image and measure it as a test (if the min and max are both 255 the threshold hasn't applied) go back and click the threshold pop-up… this should reset it. You can test it again by measuring a portion (it should now read a min of 0 and a max of 255).

9) Set what you want to measure by, Analyze → Set measurements. Select: area, integrated density, limit to threshold.
10) Circle 3-5 ROI's that cover as much of the muscle area as possible. Press ctrl+t to add them to the ROI manager
11) Measure all ROI's. highlight all ROIs and press 'measure'
12) Copy and paste measurements into excel. Ratio of integrated density/area. Take average of ratios for each sample.

<u>Image J Analysis – Myosin Heavy Chain (fibre CSA, proportions, and myonuclear characteristics)</u>

MyHC fibre type and CSA analysis Image J

- Open Image J
- Drag and drop specific ROI into image J
- Open the combined channels image as well as the images with individual channels (AF488, AF594, AF647, Cy3, and DAPI)
- Set the scale on the combined channels image using the scale bar on the specific ROI
    - o Analyze → set scale → click global → apply
- Using the freehand selection tool begin by drawing around the lamina of any Type I fibres (red)

- Then hit ‘command+m’ to measure area and subsequently ‘command+f’ to fill that specific fibre in black so you know that it has already been counted
- After measuring the area of that specific fibre type copy and paste the results into the excel spreadsheet and count how many fibres in total o Repeat this same process for Type IIA, Type IIB, and any hybrid fibres
- *note: to determine if fibres are hybrid – use the individual channel images to see if specific channels are fluorescing on the same fibre

MyHC myonuclear domain analysis image J

- Open Image J
- Drag and drop specific ROI into image J
- Open the combined channels image as well as the images with individual channels (AF488,

  AF594, AF647, Cy3, and DAPI)
- Set the scale on the combined channels image using the scale bar on the specific ROI
  - o Analyze → set scale → click global → apply
- begin with Type 1 fibres - using the freehand selection tool begin by drawing around the lamina of the first type 1 fibre and count how many nuclei are fully beneath or at least

  50% beneath the lamina
- record the number of nuclei in your excel spreadsheet in a column

- then hit ‘command+m’ to measure area and subsequently ‘command+f’ to fill that specific fibre in black so you know that it has already been counted
- proceed for the rest of the fibre types and copy and paste the final column with all CSA beside the column with the nuclei counts so that you know which area corresponds with each nuclei count